

# NMR Signatures of the Active Sites in Sn- $\beta$ Zeolite\*\*

Patrick Wolf,<sup>a,b,†</sup> Maxence Valla,<sup>a,†</sup> Aaron J. Rossini,<sup>c,†</sup> Aleix Comas-Vives,<sup>a,†</sup> Francisco Núñez-Zarur,<sup>a,†</sup> Bernard Malaman,<sup>d</sup> Anne Lesage,<sup>c</sup> Lyndon Emsley,<sup>c</sup> Christophe Copéret,<sup>a,\*</sup> Ive Hermans<sup>b,\*</sup>

**Dynamic Nuclear Polarization Surface Enhanced NMR (DNP-SENS), Mössbauer spectroscopy, and computational chemistry were combined to obtain structural information on the active-site speciation in Sn- $\beta$  zeolite. This approach unambiguously shows the presence of framework Sn<sup>IV</sup>-active sites in an octahedral environment, which probably correspond to so-called open and closed sites, respectively (namely, tin bound to three or four siloxy groups of the zeolite framework).**

Heterogeneous catalysts with well-defined isolated active sites do not only facilitate mechanistic investigations, but can also show unparalleled activity in a variety of important reactions. One example is TS-1 for the epoxidation of propene with H<sub>2</sub>O<sub>2</sub>.<sup>[1]</sup> A more recent example is Sn- $\beta$ , which consists of Sn<sup>IV</sup>-sites embedded in the zeolite- $\beta$  framework.<sup>[2]</sup> The uniform distribution of isolated Lewis acid sites, in combination with the unique hydrophobic pore architecture of the material, results in an unrivalled catalytic performance. Of particular interest is the Lewis acid-catalyzed isomerization and epimerization of sugars, key transformations in the upgrading of cellulose-based renewable feedstocks.<sup>[3]</sup> Sn- $\beta$  is also active for other reactions, including the Baeyer-Villiger oxidation of ketones and aldehydes,<sup>[4]</sup> the carbonyl-ene cyclisation of citronellal,<sup>[5]</sup> and the Meerwein-Ponndorf-Verley-Oppenauer reaction.<sup>[6]</sup> Today, Sn- $\beta$  can be

conveniently synthesized with Sn-loadings varying between 0 and 10 wt%.<sup>[7]</sup>

Despite the potential of this catalyst, the nature of its active site (distribution) is not fully determined. Various experimental investigations, including the adsorption of deuterated acetonitrile, point towards the presence of several different sites in the material, proposed as closed and open Sn<sup>IV</sup>-sites, having three and four Sn-O-Si linkages with the zeolite framework, respectively.<sup>[8]</sup> X-ray Absorption Fine Structure Spectroscopy on a 1.6 wt % sample<sup>[9]</sup> showed that Sn was located in the six-membered ring of the  $\beta$ -framework. The preferred location of Sn<sup>IV</sup> within the framework (so-called T-sites) is however still the topic of intense experimental and theoretical research.<sup>[10]</sup> Another open question is how the Sn-loading and -distribution would affect the ratio between closed and opened Sn<sup>IV</sup>-sites, and which of those sites would be active.

In principle, <sup>119</sup>Sn solid state NMR is an ideal method to probe the local structure at the Sn<sup>IV</sup>-sites. Indeed, major spectral differences have been observed between hydrated and de-hydrated samples, in particular when using isotopically enriched <sup>119</sup>Sn (due to the low Sn-loading, one typically obtains a low signal-to-noise ratio, necessitating <sup>119</sup>Sn isotopic labeling<sup>[11]</sup>). For hydrated samples, the signals observed between -685 and -736 ppm were assigned to octahedral Sn<sup>IV</sup>. Dehydrated samples are characterized by signals at much higher chemical shift (between -425 and -445 ppm), which have been proposed to correspond to tetrahedral open and closed Sn<sup>IV</sup>-sites, respectively.<sup>[12]</sup> However, the precise structure of the active sites remains unknown.

Herein we report the determination of the structure of the active sites in Sn- $\beta$  as a function of Sn-loading, by combining Mössbauer, Dynamic Nuclear Polarization Surface Enhanced NMR Spectroscopy (DNP SENS) and DFT calculations. Sn- $\beta$  zeolites with a Sn-loading ranging from 0.5 – 10 wt % were prepared *via* a two-step post-synthetic method.<sup>[7a,b]</sup> The synthesized materials were tested for the isomerization of glucose-to-fructose in water, and showed a decreasing turnover frequency (TOF) with increasing Sn-loading (Table 1), similar to what has been observed by Sels *et al.*<sup>[7c]</sup> This observation suggests the presence of distinct Sn-sites with different activities.

No major difference is observed between samples of various loadings in <sup>119</sup>Sn Mössbauer spectroscopy, performed at 300 K and 15 K (Figure S1). At 15 K, all spectra show a doublet with the hyperfine parameters, *i.e.* an isomer shift, IS  $\approx$  -0.07(3) mm/s and a quadrupole splitting, QS  $\approx$  0.75(3) mm/s (Table S1). The observed IS is consistent with a hexacoordinated Sn<sup>IV</sup> site, the large QS suggesting a distorted geometry.<sup>[13]</sup> Moreover, based on the relative increase in spectral area between 300 K and 15 K, the Sn-signals were assigned to framework sites. The small asymmetry in the experimental spectra may be due to either texture effects or the presence of minor (< 2%) additional Sn<sup>IV</sup>-sites. Note that no SnO<sub>2</sub> was detected, consistent with Diffuse Reflectance UV-Vis and Raman data, while small amounts (< 4%) of Sn<sup>II</sup> are present, presumably arising from the initial Sn<sup>II</sup> precursor used for the synthesis of Sn- $\beta$ .

For NMR in these systems, isotopic enrichment is usually required. Roy *et al.* have shown that conventional natural isotopic abundance direct polarization <sup>119</sup>Sn solid-state NMR spectra of Sn- $\beta$  can be acquired, but such experiments required between 14 to 60 hours of signal averaging for a single 1D <sup>119</sup>Sn NMR spectrum.<sup>[14]</sup>

In a DNP experiment,<sup>[15]</sup> the nuclear polarization is enhanced by microwave induced polarization transfer from unpaired electrons to nuclei (usually protons). For DNP-SENS the unpaired electrons are

[\*] a) P. Wolf, M. Valla, Dr. A. Comas-Vives, Dr. F. Núñez-Zarur, Prof. Dr. C. Copéret  
Department of Chemistry and Applied Biosciences  
ETH Zurich  
Vladimir Prelog Weg 2, Zurich, CH-8037, Switzerland  
Fax: (+41) 44-633-1315  
E-mail: [ccoperet@ethz.ch](mailto:ccoperet@ethz.ch)

b) P. Wolf, Prof. Dr. I. Hermans  
Department of Chemistry & Department of Chemical and Biological Engineering  
University of Wisconsin - Madison  
1101 University Avenue, Madison WI 53706, USA  
Fax: (+1) 608-262-8634  
E-mail: [hermans@chem.wisc.edu](mailto:hermans@chem.wisc.edu)

c) Dr. A. Rossini, Dr. A. Lesage Prof. Dr. L. Emsley  
Centre de RMN à Très Hauts Champs, Institut de Sciences Analytiques, Université de Lyon (CNRS/ENS Lyon/UCB Lyon 1), 69100 Villeurbanne, France

d) Prof. Dr. B. Malaman  
Institut Jean Lamour-CNRS-UMR 7198  
Université de Lorraine  
Faculté des Sciences BP 70239, 54506 Vandoeuvre-les-Nancy, France

† These authors have contributed equally

[\*\*] We acknowledge SNF Grants No. 200021\_143600 and 200021\_146661, Ambizione project PZ00P2\_148059, EQUIPEX contract ANR-10-EQPX-47-01, and ERC Advanced Grant No. 320860 for funding.

Supporting information for this article is available on the WWW under <http://www.angewandte.org> or from the author.

introduced by contacting the material by Incipient Wetness Impregnation with a solution of a nitroxide bi-radical, specifically often bulky 2,6-spirocyclohexyl nitroxide derivatives in tetrachloroethane solutions.<sup>[16]</sup> In the case of nanoparticulate and mesoporous samples, impregnation brings the radical solution into direct contact with the surface of the material allowing the polarization of the protons near the surface to be highly enhanced by DNP. This enhanced <sup>1</sup>H polarization is then transferred to the hetero-nuclei (e.g., <sup>13</sup>C, <sup>27</sup>Al, <sup>29</sup>Si, <sup>119</sup>Sn, etc.) at the surface.<sup>[17]</sup> Some of us recently demonstrated the rapid acquisition of natural abundance <sup>119</sup>Sn signals in core-shell ligand-capped Sn/SnO<sub>x</sub> nanoparticles using DNP SENS NMR.<sup>[18]</sup> In this work, an analogous methodology is used to investigate the molecular structure of the Sn<sup>IV</sup>-sites in Snβ.<sup>[19]</sup>

**Table 1.** Catalytic activity of Sn-β with different Sn-loadings for glucose isomerization in H<sub>2</sub>O.<sup>[a]</sup>

Entry	Catalyst	Sn loading (wt %)	TOF <sub>init</sub> <sup>[b, c]</sup> (h <sup>-1</sup> )
1	Sn-β	0.5	56±15
2	Sn-β	1	49±11
3	Sn-β	2	26±3
4	Sn-β	5	18±0.6
5	Sn-β	10	10±0.2
6	deAl-β	-	N/A <sup>[d]</sup>
7	SnO <sub>2</sub> /deAl-β	10	N/A <sup>[d]</sup>

[a] Reaction conditions: 100 mg of catalyst in 10 mL of a 5 wt % aqueous glucose solution at 373 K. [b] Defined as the mole product generated per mole Sn per hour calculated at the initial stage of the reaction. [c] Error estimated based on ICP-determined Sn-loading. [d] no product detected by HPLC after 4h of reaction.

Samples for <sup>119</sup>Sn DNP SENS were prepared by impregnating the zeolites with a 16 mM solution of TEKPo<sup>[20]</sup> in TCE. Since the pores of Sn-β are quite small (ca. 7 Å diameter), the TEKPo radical is not able to enter the material and cannot interact with the Sn-sites. The pores of the Sn-β will be filled with TCE and/or water from ambient moisture. Enhanced <sup>1</sup>H polarization will be generated at the surface of the Sn-β particles and then transported into the interior of the particles by <sup>1</sup>H spin diffusion along the channels (as previously observed for MOF samples).<sup>[21]</sup> Since the Sn-β particles are quite small (200-400 nm), high <sup>1</sup>H DNP enhancements (greater than 60, corresponding to an acceleration by a factor of 3600 in time) were obtained in all cases, enabling the rapid acquisition of natural abundance <sup>119</sup>Sn CPMAS NMR spectra even for low loading levels (0.5 wt% Sn). By comparison, the <sup>119</sup>Sn CP NMR spectra acquired without microwave irradiation, and the same number of scans showed no signal, even for high loaded samples. The total spectrometer time required to obtain all the data in Figure 1 was only 3 hours. Acquisition can be further accelerated by the application of CP-CPMG pulse sequences (Figure S2).<sup>[22]</sup>

In all spectra three isotropic Sn chemical shifts centered at ca. -614 (S3), -659 (S2) and -685 ppm (S1) were identified from both 1D CP spin echo (Figure 1) and 2D CPMAT <sup>119</sup>Sn spectra (*vide infra*). The relative intensity of these sites varies as a function of Sn-loading level (Figures 1 and S3).

Cross Polarization Magic Angle Turning (CPMAT) experiments<sup>[23]</sup> were recorded on the 5 and 1 wt% Sn-β samples. A CPMAT spectrum correlates the MAS sideband manifolds to a single isotropic chemical shift in the indirect dimension. This method allows the chemical shift anisotropy (CSA) to be measured for each <sup>119</sup>Sn site of the overlapping sideband manifolds. The Sn CSA arises from the anisotropy of the electronic distribution around the Sn nucleus.

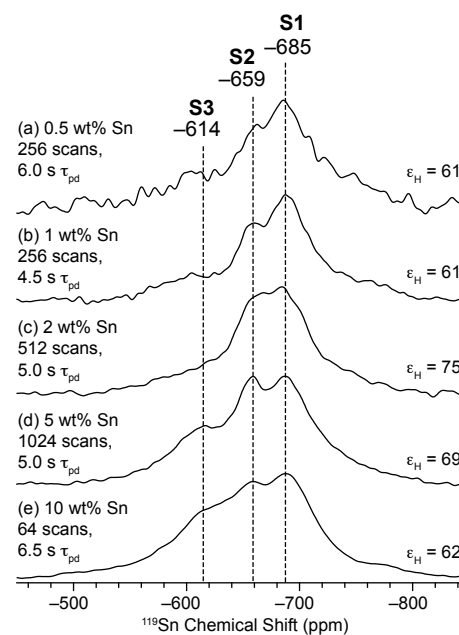


**Figure 1.** 9.4 T 105 K <sup>1</sup>H-<sup>119</sup>Sn DNP SENS magic angle spinning cross-polarization spin echo spectra of (a) 0.5 wt% Sn β-zeolite, (b) 1 wt% Sn β-zeolite, (c) 2 wt% Sn β-zeolite, (d) 5 wt% Sn β-zeolite, (e) 10 wt% Sn β-zeolite. All samples were impregnated with a 16 mM TEKPo 1,1,2,2-tetrachloroethane solutions. All spectra were acquired with a MAS frequency of 12.5 kHz and CP contact times between 3.0 and 3.5 ms. The number of scans and polarization delay ( $\tau_{pd}$ ) are indicated for each spectrum together with the proton DNP enhancements ( $\epsilon_H$ ) measured with separate <sup>1</sup>H spin echo experiments. The signals around -580 and -780 ppm, as observed for the 10 wt % sample, correspond to spinning sidebands.

CSA parameters are often described by the isotropic chemical shift ( $\delta_{iso}$ ), the span ( $\Omega$ ) and the skew ( $-1 \leq \kappa \leq +1$ ) which are calculated from the principal tensor components of the chemical shift tensor  $\delta_{11} \geq \delta_{22} \geq \delta_{33}$ :<sup>[24]</sup>

$$\bar{\delta}_{iso} = (\delta_{11} + \delta_{22} + \delta_{33})/3 \quad (1)$$

$$\Omega = (\delta_{11} - \delta_{33}) \quad (2)$$

$$\kappa = 3(\delta_{22} - \bar{\delta}_{iso})/\Omega \quad (3)$$

$\bar{\delta}_{iso}$  is the average of the three components of the CSA tensor and is analogous to the chemical shift that is observed in solution NMR.  $\Omega$  describes the magnitude of the anisotropy and reports on the degree of spherical symmetry of the electronic distribution at the nuclear site, while  $\kappa$  describes the rhombicity of the.

The 2D-CPMAT of the 5 wt% Sn-β is shown in Figure 2, where the isotropic NMR spectrum can be observed in the indirect dimension ( $F_1$ ) and the normal CP spectrum (isotropic peaks and spinning sidebands) can be observed in the direct dimension ( $F_2$ ). Fitting of the sideband manifolds extracted from the direct dimension at the position of the corresponding provides the CS tensor parameters ( $\bar{\delta}_{iso}$ ,  $\Omega$  and  $\kappa$ ). The signal S3 at -614 ppm is similar to that observed for bulk SnO<sub>2</sub>, and this site is found to have a  $\Omega$  of 162 ppm and a  $\kappa$  of +0.13, consistent with the octahedral environment of Sn in SnO<sub>2</sub>. This resonance has previously been assigned to extra-framework SnO<sub>2</sub> and is typically observed at high Sn-loadings (> 1 wt%). In addition, the two other signals at -659 (S2) and -685 ppm (S1) are associated with slightly different CSA parameters (S2:  $\Omega = 155$  ppm and  $\kappa = +0.05$  and S1:  $\Omega = 146$  ppm and  $\kappa = +0.21$ ). The chemical shifts and the skews ( $\kappa$ ) close to 0 point toward a slightly distorted octahedral Sn environments (*vide infra*). The 2D-CPMAT experiment on 1 wt% Sn-β (Figure S4) shows the two peaks at -659 ppm and -685 ppm with similar CSA parameters as observed in the 5 wt% Sn-β sample, consistent with the presence of similar species,

suggesting that increased loading does not change the nature of Sn species, but only their ratio.

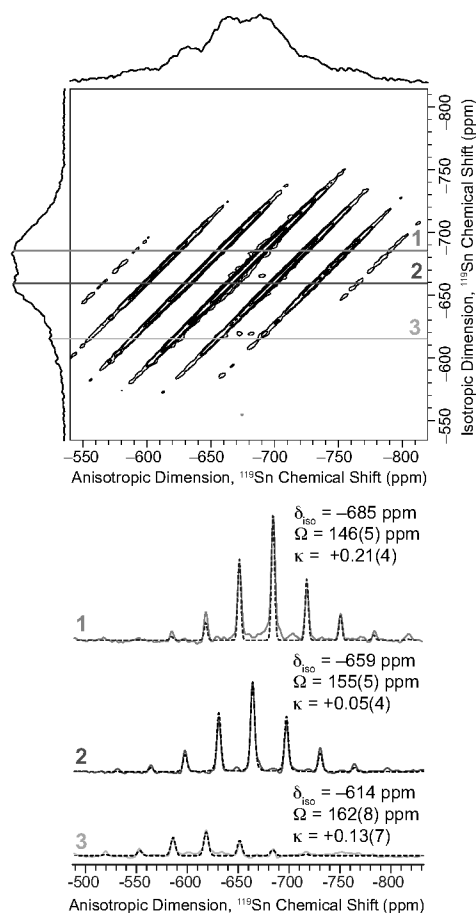


**Figure 2.** 105 K  $^{119}\text{Sn}$  DNP SENS CP Magic Angle Turning (CP-MAT) spectra of 5 wt% Sn  $\beta$ -zeolite impregnated with a 16 mM solution of TEKPol in tetrachloroethane. The spectrum was acquired on a 400 MHz DNP spectrometer, with a sample spinning frequency of 5 kHz and a polarization delay of 5 s. 512 scans per increment and 160  $t_1$  increments were acquired. A  $^1\text{H}$  DNP enhancement of ca. 85 was obtained. Spinning sideband manifolds are shown for the three different isotropic shifts and the extracted CS tensor parameters are indicated. Fits of the sideband manifolds are also shown (dashed black lines).

The one-dimensional  $^{119}\text{Sn}$  DNP SENS CPMAS spectra were deconvolved (Figure S5) and the relative ratio of each species evaluated (Table 2). Note that since DNP and CP are used to obtain the spectra, it is not possible to quantitatively evaluate the amount of each site, but that this analysis should provide an estimate of the variation of the relative ratio of each site. At low loading, Sn- $\beta$  is constituted mainly of S1, and increased loading leads to increased intensity of S3, associated with extra framework  $\text{SnO}_2$ , while the relative amount of S2 is approximately constant as a function of the loading level. Reconciling these deconvolved spectroscopic data with the catalytic activity results in Table 1 suggests that the sites associated with signals S1 and S2 are both active in the glucose-to-fructose isomerization (see Figure S6). Note that a significant amount of  $\text{SnO}_2$  is detected by DNP SENS even though it was not observed with Mössbauer, Raman and UV-Vis spectroscopies. It is therefore likely that the  $\text{SnO}_2$  clusters are located outside the zeolite framework, closer to the polarizing agent where the DNP enhancement will be higher.

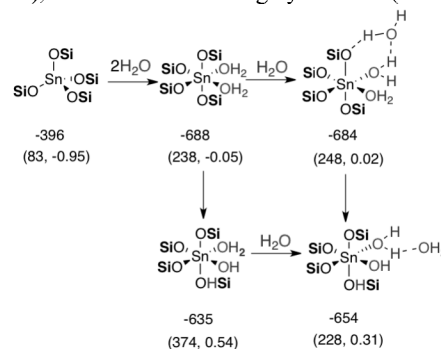
In order to relate these observations directly to the local structure of the Sn environment, DFT calculations on cluster models were carried out in order to assign the observed NMR signatures. We first used a small cluster model of the T-site in order to screen several

structural possibilities and to calibrate the methodology. Details on the models and the methodologies are given in the Supporting Information (see e.g. Table S2 for an overview of all structures which were investigated).

**Table 2.** Relative contribution of the three  $^{119}\text{Sn}$  signals (deconvoluted areas in percentage) as a function of the Sn-loading as determined from DNP SENS showing a qualitative trend in active site-distribution.

Entry	Sn-loading (wt%)	S3 (%) -614 ppm	S2 (%) -659 ppm	S1 (%) -685 ppm
1	0.5	8	27	65
2	1	8	28	64
3	2	11	36	53
4	5	16	35	49
5	10	24	29	47

For the most realistic cluster model, that includes the zeolite framework, the tetrahedral site has a calculated  $\delta_{\text{iso}}$  of  $-396$  ppm, in good agreement with experimental values (*vide supra*), and the chemical shift decreases by ca. 100 ppm with the addition of each (1 or 2) coordinated water molecule (see Supporting Information). The hexacoordinated Sn-sites, resulting from the coordination/reaction of at least two water molecules, have calculated NMR parameters consistent with the experimental values. When Sn-sites have two water molecules in the first coordination sphere and one additional water molecule H-bonded to the coordinated  $\text{H}_2\text{O}$ , the calculated NMR parameters are in very good agreement with the experimental chemical shift parameters:  $\delta_{\text{iso}}/\Omega/\kappa$  of  $-654/228/0.31$  and  $-684/248/0.02$  for opened or closed sites, respectively, allowing the assignment of S2 ( $-654$  ppm) to an opened site and S1 ( $-685$  ppm) to a closed site, coordinated by two  $\text{H}_2\text{O}$  molecules. The low  $\Omega$  and a value of  $\kappa$  close to 0 are consistent with distorted octahedral sites. In terms of stability, the T<sub>1</sub> sites with two coordinated water molecules (closed site) are energetically more favored by ca. 9 kcal mol<sup>-1</sup> than the corresponding opened site with one coordinated  $\text{H}_2\text{O}$  and one Sn-O-Si bridge opened by  $\text{H}_2\text{O}$  (Table S4). However, the presence of an additional water molecule on the second coordination sphere is crucial to stabilize the opened site structure *via* hydrogen-bonding (see Table S4), which is otherwise highly unstable (+19 kcal mol<sup>-1</sup>).



**Scheme 1.** Computed  $^{119}\text{Sn}$  isotropic chemical shifts in ppm ( $\delta_{\text{iso}}$  upper numbers outside of parenthesis). The span  $\Omega$  (in ppm) and skew  $\kappa$  are shown in parenthesis (see also Supporting Information).

In summary, combining Mössbauer spectroscopy, DNP-SENS and DFT calculations show that the active sites of Sn- $\beta$  zeolite correspond to octahedrally coordinated  $\text{Sn}^{\text{IV}}$ , involving the tetrahedral Sn-sites and two water molecules. Two types of Sn are determined here: one where two water molecules are coordinated to Sn (closed site), and another where one of the water molecules has opened one of the Sn-O-Si bridges (opened site). These two species, with distinct NMR signatures, are the active sites of Sn- $\beta$  zeolite.

## Experimental Section

Sn- $\beta$  samples were synthesized and characterized as described elsewhere.<sup>[7a]</sup> Glucose isomerization reactions in H<sub>2</sub>O were carried out in a 25 mL sealed round bottom flask. The vessel was charged with 10 mL of 5 wt% aqueous glucose solution and heated to 100 °C for 15 min, prior to the addition of 100 mg of catalyst. The reaction mixture was stirred vigorously at 500 rpm for the required reaction period. Samples were taken periodically and quantified by HPLC equipped with an RI detector. Monosaccharides were separated using a Ca<sup>2+</sup> column (Phenomenex).

<sup>119</sup>Sn Mössbauer measurements were carried out using a constant-acceleration spectrometer in standard transmission geometry with a Ba<sup>119m</sup>SnO<sub>3</sub> source (10 mCi) kept at room temperature as a reference for the isomer shifts. Spectra of each sample were recorded at 300 and 15 K in a liquid helium cryostat. The velocity scale was calibrated with a <sup>57</sup>CoRh source (25 mCi) and a metallic iron foil at room temperature. A polycrystalline absorber with natural abundance of <sup>119</sup>Sn isotope and thickness of 15 mg cm<sup>-2</sup> was used. A palladium foil of 0.5 mm thickness was used as a critical absorber for tin X-rays. The Mössbauer spectra were fitted by using a unique doublet with a FWHM value of around 1.0 mm/s (see Table S1) with a least-squares method program assuming Lorentzian.<sup>[25]</sup>

DNP solid-state NMR experiments were performed on a Bruker Avance III 9.4 T (400 MHz/263 GHz <sup>1</sup>H/electron Larmor frequencies) DNP spectrometer<sup>[26]</sup> equipped with a gyrotron microwave source. The sweep coil of the main superconducting NMR coil was set so that microwave irradiation occurred at the positive enhancement maximum for the TOTAPOL biradical.<sup>[27]</sup> Samples were prepared for DNP SENS experiments by applying incipient wetness impregnation with a 16 mM solution of the TEKPol<sup>[20]</sup> biradical in 1,1,2,2-tetrachloroethane to the Sn  $\beta$ -zeolite materials. Typically 25 mg of material was impregnated with 20  $\mu$ L of biradical solution then packed into 3.2 mm outer diameter sapphire rotors. The <sup>119</sup>Sn spectra were acquired with a rotor synchronized CP spin echo pulse sequence and the full spin echo signal was acquired. CP experiments were typically performed with a 2.5  $\mu$ s <sup>1</sup>H  $\pi/2$  pulse for excitation and <sup>1</sup>H and <sup>119</sup>Sn spin lock rf fields of ca. 72 kHz and MAS frequencies of 12.5 kHz. The amplitude of the <sup>1</sup>H spin lock pulse was linearly ramped from 90 to 100% of its maximum value. Optimized contact times of 3.0 to 3.5 ms were used. SPINAL-64 heteronuclear <sup>1</sup>H decoupling was applied in all experiments.<sup>[27]</sup> The constant time five- $\pi$  pulse MAT experiment of Grant and co-workers was employed for acquisition of the 2D <sup>119</sup>Sn chemical shift correlation spectra.<sup>[23]</sup> CS tensor parameters were obtained by fitting the sideband manifolds with the HBA-Graphic Analysis Program v1.7.3 (Dr. K. Eichele, University of Tübingen).

Received: ((will be filled in by the editorial staff))

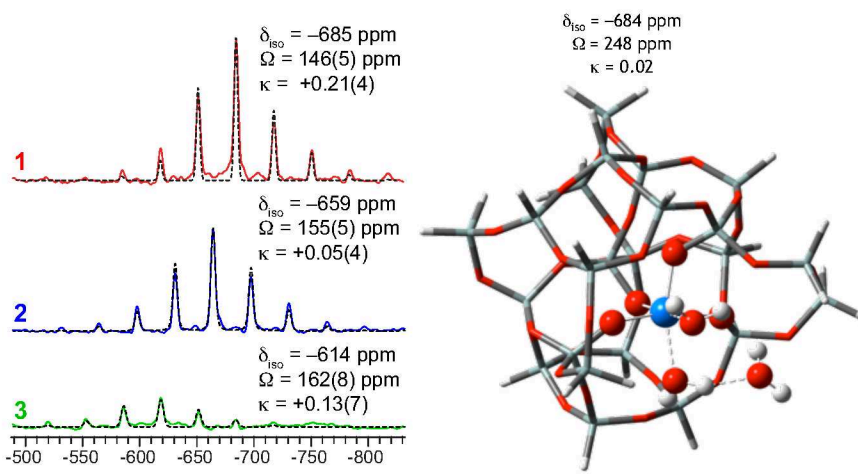
Published online on ((will be filled in by the editorial staff))

**Keywords:** Sn- $\beta$  · zeolite · Mössbauer · solid-state NMR · DNP SENS · active sites · DFT

- [1] a) F. Cavani, J. H. Teles, *ChemSusChem* **2009**, *2*, 508-534; b) Notari *Adv. Catal.* **1996**, *41*, 253-334; c) S. Bordiga, A. Damin, F. Bonino, C. Lamberti, in *Surface and Interfacial Organometallic Chemistry and Catalysis*, Vol. 16 (Eds. C. Copéret, B. Chaudret), Springer-Verlag Berlin, Heidelberg, **2005**, pp. 37-68.
- [2] Y. Román-Leshkov, M. Davis, *ACS Catalysis* **2011**, *1*, 1566-1580; b) R. Lobo, *AIChE J.* **2008**, *54*, 1402-1409; c) M. Dusselier, P. Van Wouwe, A. Dewaele, E. Makshina, B. F. Sels, *Energy Environ. Sci.* **2013**, *6*, 1415-1442.
- [3] a) M. S. Holm, S. Saravanamurugan, E. Taarning, *Science* **2010**, *328*, 602-603; b) Y. Román-Leshkov, M. Moliner, J. A. Labinger, M. E. Davis, *Angew. Chem. Int. Ed.* **2010**, *49*, 8954-8957; c) M. Moliner, Y. Román-Leshkov, M. E. Davis, *Proc. Natl. Acad. Sci. U.S.A.* **2010**, *107*, 6164-6168; d) W. R. Gunther, Y. Wang, Y. Ji, V. K. Michaelis, S. T. Hunt, R. G. Griffin, Y. Román-Leshkov, *Nature Communications* **2012**, *3*, 1109-1116.
- [4] a) A. Corma, L. Nemeth, M. Renz, S. Valencia, *Nature* **2001**, *412*, 423-425; b) A. Corma, V. Fornés, S. Iborra, M. Mifsud, M. Renz, *J. Catal.* **2004**, *221*, 67-76; c) M. Renz, T. Blasco, A. Corma, V. Fornés, R. Jensen, L. Nemeth, *Chem. Eur. J.* **2002**, *8*, 4708-4717
- [5] A. Corma, M. Renz, *Chem. Comm.* **2004**, 550-551.
- [6] a) A. Corma, M. E. Domine, L. Nemeth, S. Valencia, *J. Am. Chem. Soc.* **2002**, *124*, 3194-3195; b) M. Boronat, A. Corma, M. Renz, *J. Phys. Chem. B* **2006**, *110*, 21168-21174; c) A. Corma, M. E. Domine, S. Valencia, *J. Catal.* **2003**, *215*, 294-304.
- [7] a) C. Hammond, S. Conrad, I. Hermans, *Angew. Chem. Int. Ed.* **2012**, *51*, 11736-11739; b) P. Wolf, C. Hammond, S. Conrad, I. Hermans, *Dalton Transactions* **2014**, *43*, 4514-4519; c) J. Dijkmans, D. Gabriëls, M. Dusselier, F. de Clippel, P. Vanelderden, K. Houthoofd, A. Malfliet, Y. Pontikes, B. F. Sels, *Green Chemistry* **2013**, *15*, 2777-2785; d) P. Li, G. Liu, H. Wu, Y. Liu, J. Jiang, P. Wu, *J. Phys. Chem. C* **2011**, *115*, 3663-3670.
- [8] a) M. Boronat, P. Concepción, A. Corma, M. Renz, S. Valencia *J. Catal.* **2005**, *234*, 111-118; b) M. Boronat, P. Concepción, A. Corma, M. Renz, *Catalysis Today* **2007**, *121*, 39-44.
- [9] S. R. Bare, S. D. Kelly, W. Sinkler, J. J. Low, F. S. Modica, S. Valencia, A. Corma, L. T. Nemeth, *J. Am. Chem. Soc.* **2005**, *127*, 12924-12932.
- [10] a) G. Yang, E. Pidko, E. J. M. Hensen, *J. Phys. Chem. C* **2013**, *117*, 3976-3986, b) G. Yang, E. A. Pidko, E. J. M. Hensen, *ChemSusChem* **2013**, *6*, 1688-1696.
- [11] R. Bermejo-Deval, R. S. Assary, E. Nikolla, M. Moliner, Y. Román-Leshkov, S.-J. Hwang, A. Palsdottir, D. Silverman, R. F. Lobo, L. A. Curtiss, M. E. Davis, *Proc. Natl. Acad. Sci. U.S.A.* **2012**, *109*, 9727-9732.
- [12] R. Bermejo-Deval, R. Gounder, M. E. Davis, *ACS Catalysis* **2012**, *2*, 2705-2713.
- [13] Tetrahedral Sn<sup>IV</sup> is expected with significant negative value (IS=-0.2 mm/s), corroborating the hexacoordination of Sn in the sample; Parish, R.V. in *Mössbauer Spectroscopy Applied to Inorganic Chemistry*, Vol. 1 (Ed. G.J. Long) Plenum Press, New York, 1984, p. 527.
- [14] S. Roy, K. Bakhmutsky, E. Mahmoud, R. F. Lobo, R. J. Gorte, *ACS Catal.* **2013**, *3*, 573-580.
- [15] T. Maly, G. T. Debelouchina, V. S. Bajaj, K. N. Hu, C. G. Joo, M. L. Mak-Jurkauskas, J. R. Sirigiri, P. C. A. van der Wel, J. Herzfeld, R. J. Temkin, R. G. Griffin, *J. Chem. Phys.* **2008**, *128*, 052211.
- [16] a) A. Zagdoun, A. J. Rossini, D. Gajan, A. Bourdolle, O. Ouari, M. Rosay, W. E. Maas, P. Tordo, M. Lelli, L. Emsley, A. Lesage, C. Copéret *Chem. Commun.* **2012**, *48*, 654-656; b) A. Zagdoun, G. Casano, O. Ouari, G. Lapadula, A. Rossini, M. Lelli, M. Baffert, D. Gajan, L. Veyre, W. Maas, M. Rosay, R. Weber, C. Thieuleux, C. Coperet, A. Lesage, P. Tordo, L. Emsley *J. Am. Chem. Soc.* **2012**, *134*, 2284-2291; c) D. Gajan, M. Schwarzwälder, M. P. Conley, W. R. Gruening, A. J. Rossini, A. Zagdoun, M. Lelli, M. Yulikov, G. Jeschke, C. Sauvée, O. Ouari, P. Tordo, L. Veyre, A. Lesage, C. Thieuleux, L. Emsley, C. Copéret, *J. Am. Chem. Soc.* **2013**, *135*, 15459-15466.
- [17] a) A. Lesage, M. Lelli, D. Gajan, M. A. Caporini, V. Vitzthum, P. Miéville, J. Alauzun, A. Roussey, C. Thieuleux, A. Mehdi, G. Bodenhausen, C. Copéret, L. Emsley, *J. Am. Chem. Soc.* **2010**, *132*, 15459-15461; b) M. Lelli, D. Gajan, A. Lesage, M. A. Caporini, V. Vitzthum, P. Miéville, F. Héroguel, F. Rascon, A. Roussey, C. Thieuleux, M. Boualleg, L. Veyre, G. Bodenhausen, C. Copéret, and L. Emsley, *J. Am. Chem. Soc.* **2011**, *133*, 2104-2107; c) A. Rossini, A. Zagdoun, M. Lelli, A. Lesage, C. Copéret, L. Emsley, *Acc. Chem. Res.* **2013**, *46*, 1942-1951.
- [18] L. Protesescu, A. J. Rossini, D. Kriegner, M. Valla, A. de Kergommeaux, M. Walter, K. V. Kravchik, M. Nachttegaal, J. Stangl, B. Malaman, P. Reiss, A. Lesage, L. Emsley, C. C. Copéret, M. V. Kovalenko, *ACS Nano* **2014**, *8*, 2639-2648.
- [19] After submission of this manuscript the following paper appeared on the use of DNP enhanced <sup>119</sup>Sn NMR for hydrothermally synthesized Sn $\beta$ : W. R. Gunther, V. K. Michaelis, M. A. Caporini, R. G. Griffin, Y. Román-Leshkov, *J. Am. Chem. Soc.* **2014**, *136*, 6219-6222.
- [20] A. Zagdoun, G. Casano, O. Ouari, M. Schwarzwälder, A. J. Rossini, F. Aussenac, M. Yulikov, G. Jeschke, C. Copéret, A. Lesage, P. Tordo, L. Emsley, *J. Am. Chem. Soc.* **2013**, *135*, 12790-12797.
- [21] a) P. C. A. van der Wel, K. N. Hu, J. Lewandowski, R. G. Griffin, *J. Am. Chem. Soc.* **2006**, *128*, 10840-10846; b) A. J. Rossini, A. Zagdoun, F. S. Hegner, M. Schwarzwälder, D. Gajan, C. Copéret, A. Lesage, L. Emsley, *J. Am. Chem. Soc.* **2012**, *134*, 16899-16908; c) O. Lafon, A.

- S. L. Thankamony, T. Kobayashi, D. Carnevale, V. Vitzthum, I. Slowing, K. Kandel, H. Vezin, J. P. Amoureux, G. Bodenhausen, M. Pruski, *J. Phys. Chem. C* **2013**, *117*, 1375-1382; d) A. J. Rossini, A. Zagdoun, M. Lelli, J. Canivet, S. Aguado, O. Ouari, M. Rosay, W. E. Maas, C. Copéret, D. Farrusseng, L. Emsley, A. Lesage, *Angew. Chem. Int. Ed.* **2012**, *51*, 123-127.
- [22] A. J. Rossini, A. Zagdoun, M. Lelli, D. Gajan, F. Rascón, M. Rosay, W. E. Maas, C. Copéret, A. Lesage, L. Emsley, *Chem. Sci.* **2012**, *3*, 108-115.
- [23] J. Z. Hu, W. Wang, F. Liu, M. S. Solum, D. W. Alderman, R. J. Pugmire, D. M. Grant, *J. Magn. Reson. Ser. A* **1995**, *113*, 210-222.
- [24] J. Herzfeld, A. E. Berger, *J. Chem. Phys.* **1980**, *73*, 6021.
- [25] G. Le Caër, private communication.
- [26] M. Rosay, L. Tometich, S. Pawsey, R. Bader, R. Schauwecker, M. Blank, P. M. Borchard, S. R. Cauffman, K. L. Felch, R. T. Weber, R. J. Temkin, R. G. Griffin, W. E. Maas, *Phys. Chem. Chem. Phys.* **2010**, *12*, 5850-5860.
- [27] B. M. Fung, A. K. Khitrin, K. J. Ermolaev, *J. Magn. Reson.* **2000**, *142*, 97-101.
-

## Entry for the Table of Contents

Active Sites in Sn- $\beta$	DNP-CP-MAT      DFT Calculations
P. Wolf, M. Valla, A. J. Rossini, A. Comas-Vives, F. Núñez-Zarur, B. Malaman, <sup>d</sup> A. Lesage, <sup>c</sup> L. Emsley, <sup>c</sup> C. Copéret, <sup>a,*</sup> I. Hermans <sup>b,*</sup> _____ <b>Page – Page</b>	 <p><b>1</b> <math>\delta_{iso} = -685</math> ppm <math>\Omega = 146(5)</math> ppm <math>\kappa = +0.21(4)</math></p> <p><b>2</b> <math>\delta_{iso} = -659</math> ppm <math>\Omega = 155(5)</math> ppm <math>\kappa = +0.05(4)</math></p> <p><b>3</b> <math>\delta_{iso} = -614</math> ppm <math>\Omega = 162(8)</math> ppm <math>\kappa = +0.13(7)</math></p> <p>Anisotropic Dimension, <math>^{119}\text{Sn}</math> Chemical Shift (ppm)</p> <p><b>Octahedral Sn site</b></p>
NMR Signatures of the Active Sites in Sn- $\beta$ Zeolite	<p><b>Open or close:</b> the spectroscopic signatures of Sn-<math>\beta</math> obtained through <math>^{119}\text{Sn}</math> Mössbauer, and DNP-SENS combined with DFT calculations on a <math>T_1</math> site model indicate that the active sites correspond to octahedral Sn(IV) sites, where two water molecules are bound to a framework Sn.</p>

# Supporting information

## Table of contents

1. General information	S3
2. Synthesis and characterization of Iridium(I) based NHC material	S4
3. Synthesis and characterization of [IrCl(COD)(MesImPr)] <b>1</b>	S8
4. X-Ray determination of <b>1</b> [IrCl(COD)(MesImPr)]	S10
5. TEM pictures of M-Ir and corresponding EDX analyses	S13
6. Synthesis and characterization of <sup>13</sup> C labelled materials	S14
7. Characterization of Iridium(I) based NHC material by DNP method	S18
8. NMR experiments under H <sub>2</sub> pressure for COD concentration determination	S22
9. Procedures for catalytic experiments with homogeneous [IrCl(COD)(MesImPr)] and heterogeneous Iridium(I) based NHC catalysts	S26



## 1. General information.

All the reactions related to surface-modifications and synthesis of [IrCl(COD)(MesImPr)] were carried out under Ar using standard Schlenk techniques and dry degassed solvents. Mesitylimidazole and AgOC(CF<sub>3</sub>)<sub>3</sub> were synthesized in our laboratory according to the literature procedure.<sup>[1]</sup> TEOS (tetraethylorthosilicate), HI, Ag<sub>2</sub>O, Pluronic123, TMSBr were bought from Sigma-Aldrich. TEOS was distilled over Mg before use. The metal complex [IrCl(COD)]<sub>2</sub> was received from Strem Chemicals and used without further purification.

Elemental analyses were performed under inert atmosphere at the Mikroanalytisches Labor Pascher, Remagen, Germany.

Liquid state NMR spectra were recorded using a Bruker AC 300MHz (for catalysis) and 400MHz (for NMR experiments under H<sub>2</sub> pressure). MAS NMR spectra were recorded on a Bruker Advance 300 MHz spectrometer (for <sup>29</sup>Si NMR) and 500 MHz spectrometer (for <sup>1</sup>H, <sup>13</sup>C NMR) with a conventional double resonance 4 mm CP-MAS probe. The MAS frequency was set to 10 kHz for all the <sup>1</sup>H and <sup>13</sup>C experiments reported here and 5 kHz for <sup>29</sup>Si NMR. The analysis performed with a 4 mm probe.

## 2. Synthesis and characterization of Iridium(I) based NHC material

**Synthesis of Material M-Ir.** 2.6 g of protected material prepared as previously described,<sup>[1]</sup> was mixed with 0.782 g of  $\text{AgOC}(\text{CF}_3)_3$  in glove box in the absence of light and dissolved in 45 ml of dried and degassed  $\text{CH}_3\text{CN}$ . The mixture was left for stirring overnight at 25 °C. The solid was filtered under Ar and washed 3 times by degassed and dried  $\text{CH}_3\text{CN}$  (20 ml) and  $\text{CH}_2\text{Cl}_2$  (20 ml). The material was dried at 25 °C under the vacuum overnight. A brownish powder (2.5 g), **M-Ag**, was obtained and stored in glove box. Elemental Analysis: 0.72 % N; 4.27 % Ag; 36.8 % Si.

500 mg (0.17 mmol) of dried silver material, **M-Ag**, was mixed with 420 mg (1.25mmol) of  $[\text{IrCl}(\text{COD})]_2$  in glove box. Mixture was dissolved in 20 ml of dried and degassed  $\text{CH}_3\text{CN}$  and left for stirring for 48 h at 60 °C. The powder was filtered under Ar and washed with dried and degassed  $\text{CH}_3\text{CN}$  (20 ml) and  $\text{CH}_2\text{Cl}_2$  (20 ml). Elemental Analysis: 0.79 % N; 33.7 % Si; 3.91 % Ag; 2.57 % Ir. The powder was characterized by TEM, X-ray diffraction and  $^1\text{H}$ ,  $^{13}\text{C}$  and  $^{29}\text{Si}$  NMR spectroscopy.

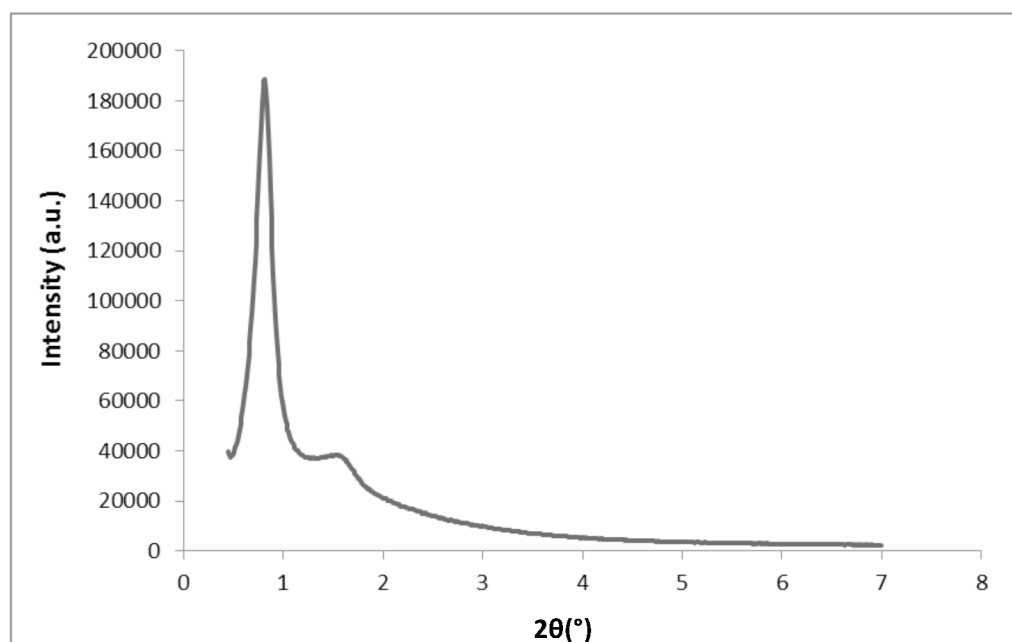


**Figure S1.** XRD pattern of **M-Ir**. The pattern exhibits an intense peak at  $2\theta = 0.82^\circ$  ( $d = 98 \text{ \AA}$  and  $a = 55 \text{ \AA}$ ).

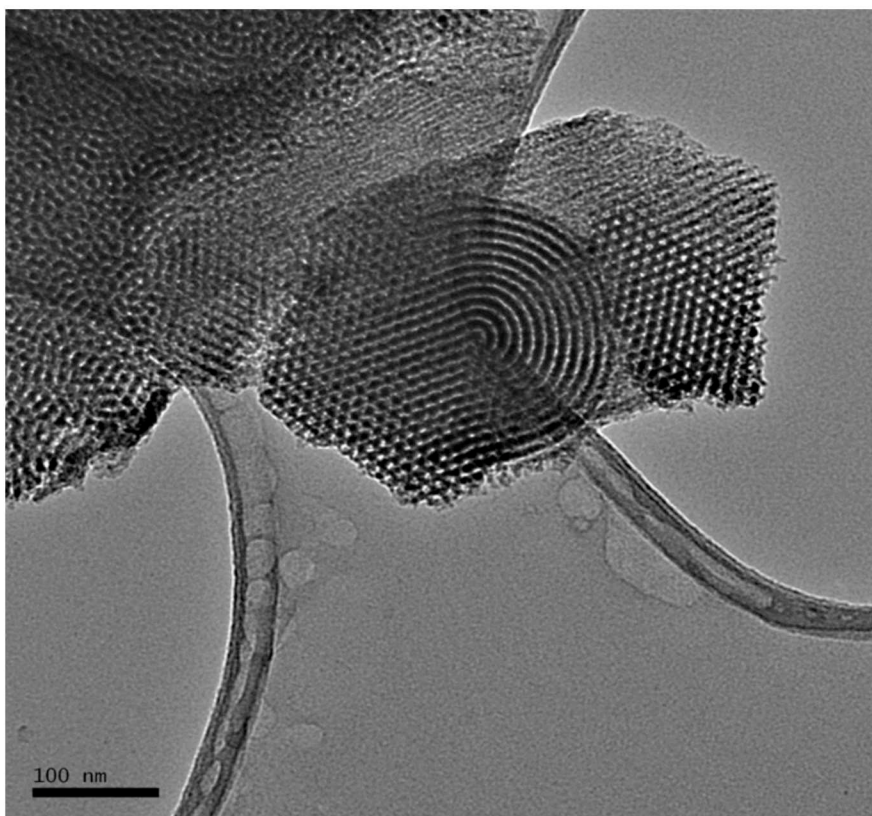


**Figure S2.** TEM micrograph of **M-Ir**. Material retains hexagonal symmetry after transmetallation.

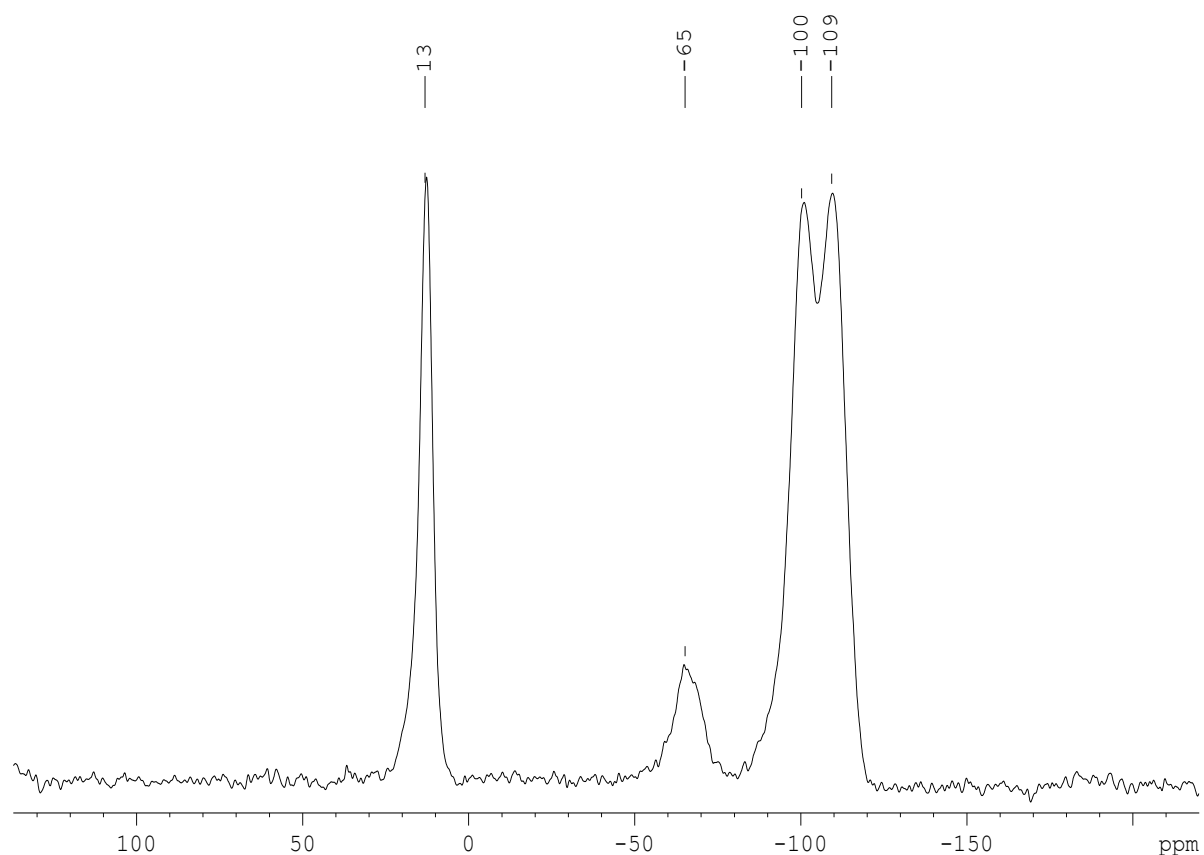


**Figure S3.**  $^{29}\text{Si}$  CP-MAS NMR spectra **M-Ir** material. The peak at 13 ppm is attributed to surface TMS (Si-OTMS), at -65 ppm to T3 site (organic moieties perfectly incorporated in the silica matrix), and at -100 ppm and -109 ppm to Q3 and Q4 (silica matrix), respectively. To be more accurate, the peak at -100 ppm can be attributed to a Q4' corresponding to the passivation of Q3 site.. The spectrum was recorded at 300 MHz (proton frequency), with a spinning frequency of 5 kHz. A total of 30000 scans with recycle delay 2 seconds were accumulated.

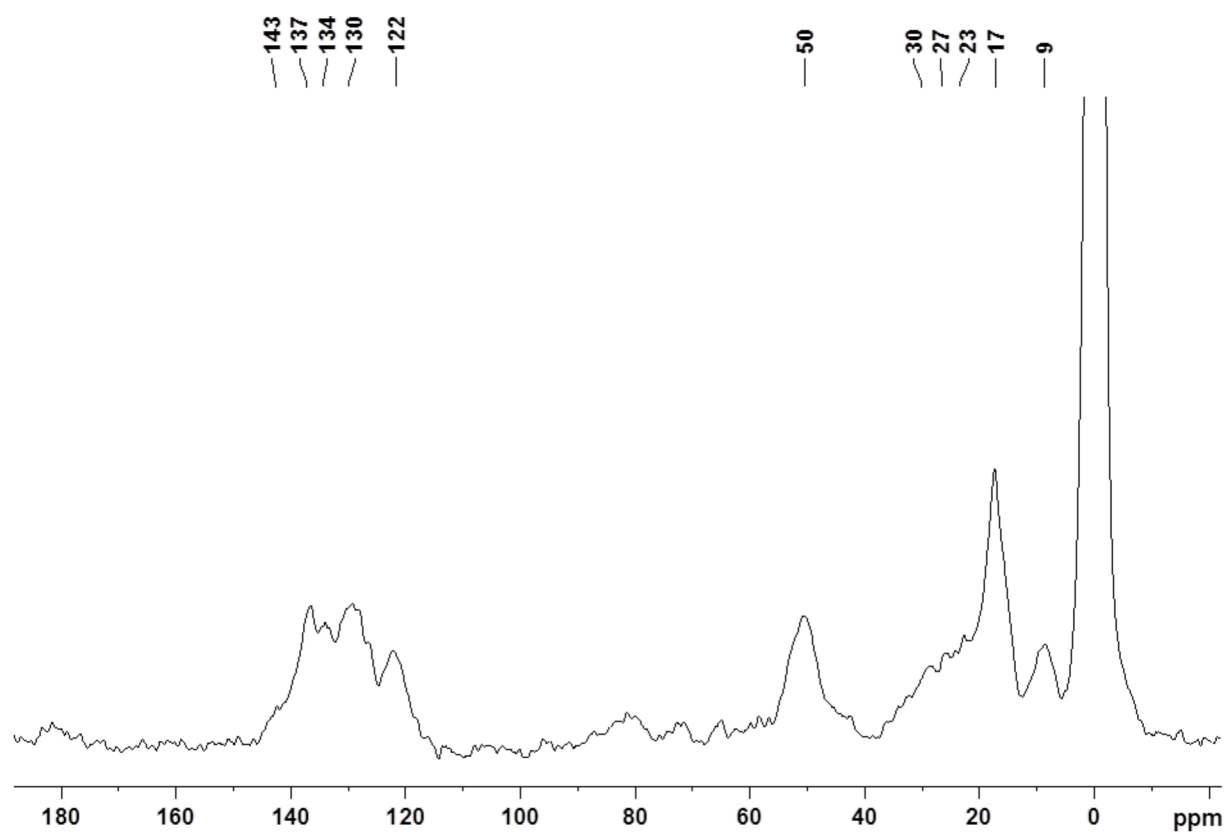


**Figure S4.**  $^{13}\text{C}$  CP-MAS NMR spectrum of M-Ir material. Peaks at 120-140 ppm are attributed to aromatic carbons, 51 ppm for  $\text{NCH}_2$ , 20 ppm for  $\text{CH}_3$  of mesityl and  $\text{SiCH}_2\text{CH}_2$ , 10 ppm for  $\text{SiCH}_2$  and 0 ppm for  $\text{Si-OTMS}$ . Signal at 61 ppm attributed to residual  $\text{SiOEt}$  groups. 184320 scans with a recycle delay 2 seconds were accumulated at 12.5 kHz.

### 3. Synthesis and characterization of [IrCl(COD)(MesImPr)] **1**

200 mg (0.6 mmol) of dried MesImPrI were mixed with 67 mg (0.3 mmol) of Ag<sub>2</sub>O in argon atmosphere in the absence of light. The mixture was dissolved in 20 ml of dried CH<sub>3</sub>CN and left for stirring at 25 °C for 4 h. Then the rest of Ag<sub>2</sub>O was filtered under inert conditions and transparent filtrate was evaporated under vacuum. The silver carbene was characterized by <sup>1</sup>H, <sup>13</sup>C NMR spectroscopy. 195 mg (0.3 mmol) of [Ir(COD)Cl]<sub>2</sub> were dissolved in 20 ml of dried and degassed CH<sub>3</sub>CN and transferred by cannula system to the silver carbene. The reaction was carried out at 60 °C during 12 h (time of reaction less than 5 h gives a mixture of products). The product was purified by column chromatography, using CH<sub>2</sub>Cl<sub>2</sub> as eluent. The orange crystals of **1** were obtained by crystallization at -28 °C from CH<sub>2</sub>Cl<sub>2</sub>. The complex **1** was characterized by <sup>1</sup>H, <sup>13</sup>C, <sup>13</sup>C dept135 and 2D <sup>1</sup>H-<sup>1</sup>H, <sup>1</sup>H-<sup>13</sup>C NMR spectroscopy, ESI-MS and X-Ray diffraction.

#### <sup>1</sup>H, <sup>13</sup>C NMR of [(MesImPr)AgI]

<sup>1</sup>H NMR (C<sub>6</sub>D<sub>6</sub>, 300K): δ (ppm)= 0.62 (t, J=7.4 Hz, 3H, CH<sub>3</sub> of Pr); 1.36 (sext., J=7.1 Hz, 2H, NCH<sub>2</sub>CH<sub>2</sub> of Pr); 1.83 (s, 6H, CH<sub>3</sub> of Mes); 2.06 (s, 3H, CH<sub>3</sub> of Mes); 3.69 (t, J=6.9 Hz, 2H, NCH<sub>2</sub> of Pr); 5.90 (s, 1H, CH of Im); 6.09 (s, 1H, CH of Im); 6.65 (s, 2H, CH of Mes).

<sup>13</sup>C NMR (C<sub>6</sub>D<sub>6</sub>, 300K): δ (ppm)=10.87 (CH<sub>3</sub> of Pr); 17.82 (2CH<sub>3</sub> of Mes); 20.99 (CH<sub>3</sub> of Mes); 24.59 (NCH<sub>2</sub>CH<sub>2</sub> of Pr); 52.84 (NCH<sub>2</sub> of Pr); 121.27(CH of Im); 120.31 (CH of Im); 129.34 (2CH of Mes); 134.92 (2C quat. of Mes); 136.17(C quat. of Mes), 138.67 (C quat. of Mes); 186.47 (C-Ag, Im).

#### <sup>1</sup>H, <sup>13</sup>C NMR of [IrCl(COD)(MesImPr)] complex **1**

<sup>1</sup>H NMR (C<sub>6</sub>D<sub>6</sub>, 300K): δ (ppm)=0.78 (t, J=7.4 Hz, 3H, CH<sub>3</sub> of Pr); 1.25-1.45(m, 1H, CH<sub>2</sub> of COD ), 1.50-1.65 (m, 5H, CH<sub>2</sub> of COD); 1.73 (s, 3H, CH<sub>3</sub> of Mes); 1,75-1.98 (m, 3H, CH<sub>2</sub> of COD); 1,98-2.09 (m, 1H, CH<sub>2</sub> of COD); 2.11 (s, 3H, CH<sub>3</sub> of Mes); 2.56 (s, 3H, CH<sub>3</sub> of Mes); 2.91 (ddd, J=13.0 Hz, J=8.1 Hz, J=7.1 Hz, 1H, =CH of COD); 3.14 (ddd, J=13.0 Hz, J=8.1 Hz, J=7.1 Hz, 1H, =CH of COD); 3.99 (td, J=7.1 Hz, J=2.5 Hz, 1H, NCH<sub>2</sub> of Pr); 4.80 (td, J=7.1 Hz, J=2.5 Hz, 1H, NCH<sub>2</sub> of Pr); 4.90-5.10 (m, 2H, =CH of COD); 5.91 (d, J=2.0Hz, 1H, CH of Im); 6.18 (d, 1H, CH of Im); 6.68 (s, 1H, CH of Mes); 6.77 (s, 1H, CH of Mes).

$^{13}\text{C}$  NMR ( $\text{C}_6\text{D}_6$ , 300K):  $\delta$  (ppm)=11.21 ( $\text{CH}_3$  of Pr); 17.51 ( $\text{CH}_3$  of Mes), 19.96 ( $\text{CH}_3$  of Mes); 20.85 ( $\text{CH}_3$  of Mes); 23.80 ( $\text{NCH}_2\text{CH}_2$ , Pr); 29.33 ( $\text{CH}_2$  of COD); 29.90 ( $\text{CH}_2$  of COD); 33.44 ( $\text{CH}_2$  of COD); 35.02 ( $\text{CH}_2$  of COD); 50.95 ( $=\text{CH}$  of COD); 50.17 ( $=\text{CH}$  of COD); 53.12 ( $\text{NCH}_2$  of Pr); 83.22 (2CH of COD); 122.37 (CH of Im), 120.60 (CH of Im); 129.84 (CH of Mes); 134.37 (C quat. of Mes); 136.53 (C quat. of Mes); 137.51 (C quat. of Mes); 138.30 (C quat. of Mes); 180.60 (C-Ir, Im).

HRMS (ESI+): calculated for  $[(\text{MesImPr})\text{Ir}(\text{Cod})(\text{CH}_3\text{CN})]^+$  ( $[\text{M}-\text{Cl} + \text{CH}_3\text{CN}]$ ) 570.2; found 570.2 .

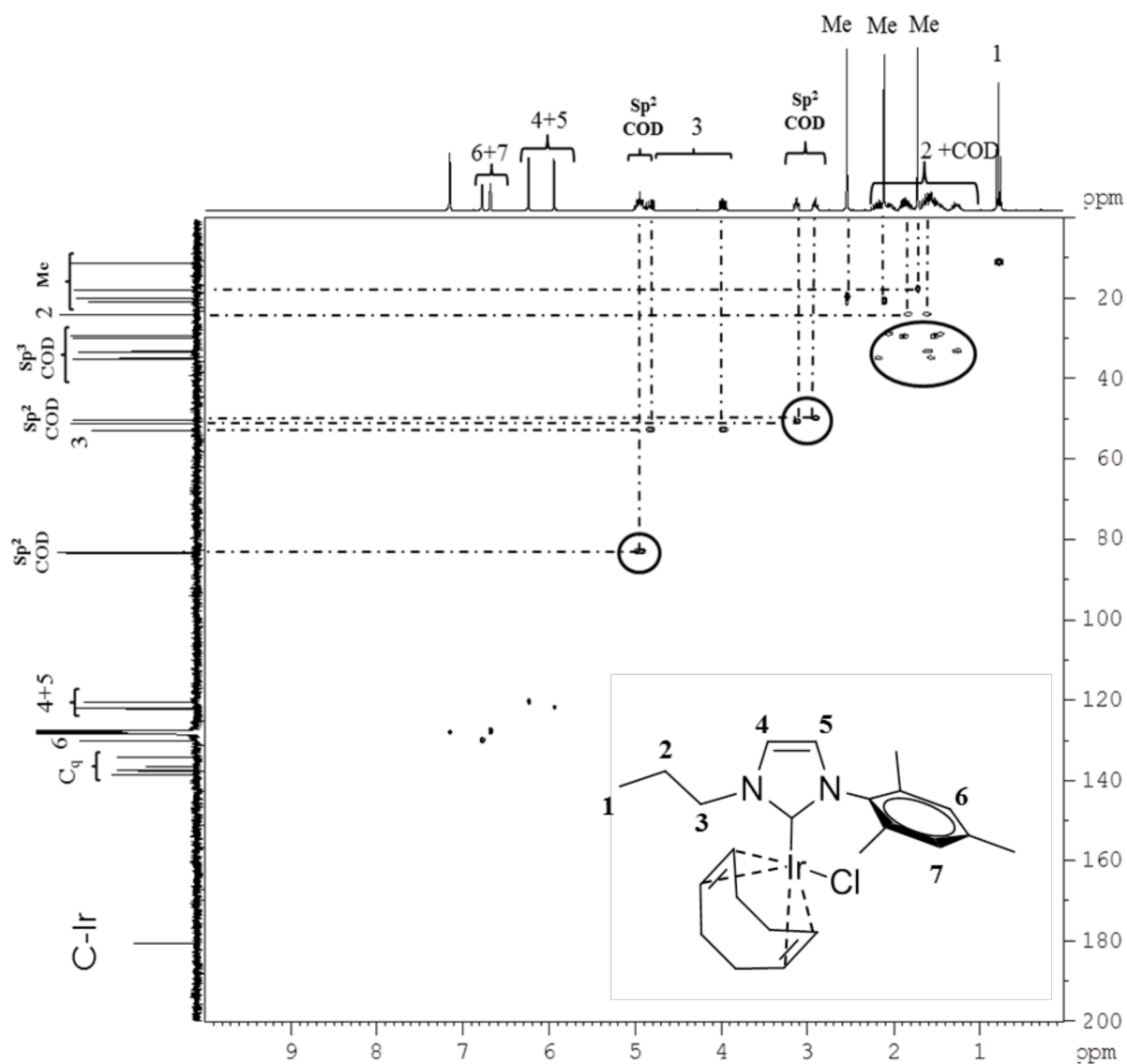


**Figure S5.**  $^1\text{H} - ^{13}\text{C}$  HMQC NMR spectrum of  $[\text{IrCl}(\text{COD})(\text{MesImPr})]$  **1** in  $\text{C}_6\text{D}_6$ . Correlations corresponding to COD are encircled.

#### 4. X-Ray diffraction analysis of **1**

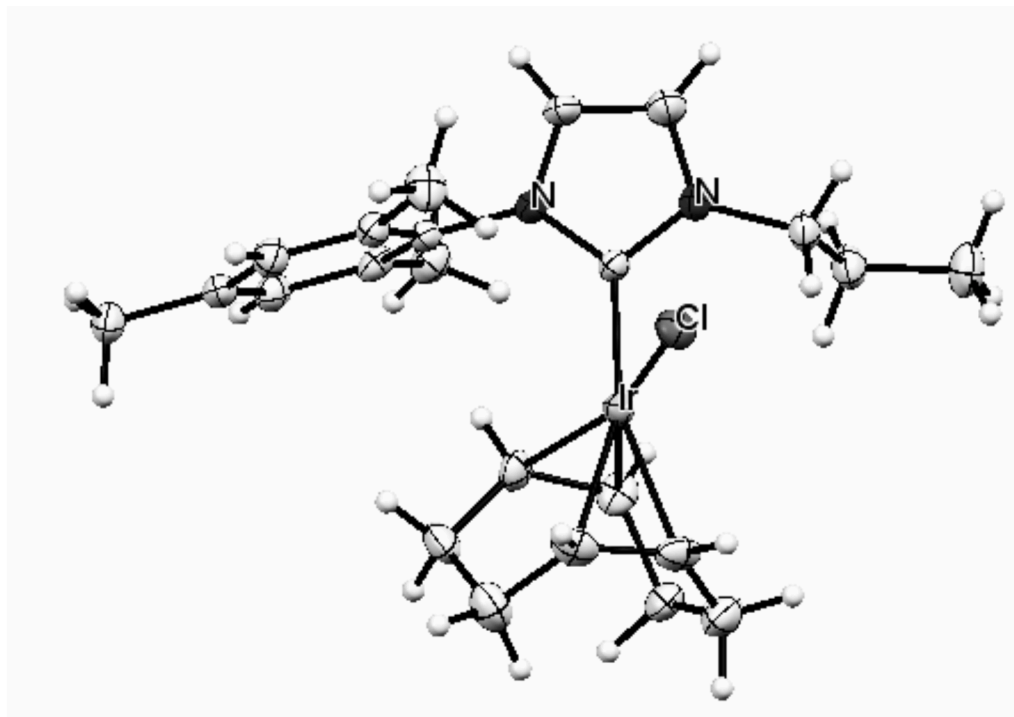


**Figure S6.** Crystal structure of **1** defined by X-Ray diffraction (CCDC 1043116)

**Table S1.** Crystal data structure refinement for **1**.

$\text{C}_{23}\text{H}_{32}\text{ClIrN}_2$	$Z = 2$
$M_r = 564.19$	$F(000) = 556$
Triclinic, $P\bar{1}$	$D_x = 1.731 \text{ Mg m}^{-3}$
Hall symbol: $-P\ 1$	Mo $K\alpha$ radiation, $\lambda = 0.7107 \text{ \AA}$
$a = 9.9815 (3) \text{ \AA}$	Cell parameters from 10034 reflections
$b = 10.2821 (3) \text{ \AA}$	$\theta = 3.7\text{--}29.0^\circ$
$c = 11.5971 (4) \text{ \AA}$	$\mu = 6.30 \text{ mm}^{-1}$
$a = 97.793 (3)^\circ$	$T = 150 \text{ K}$
$b = 95.183 (3)^\circ$	Needle, yellow
$g = 111.720 (3)^\circ$	$0.82 \times 0.45 \times 0.30 \text{ mm}$
$V = 1082.66 (7) \text{ \AA}^3$	

#### Data collection



Xcalibur, Eos, Nova diffractometer	5218 independent reflections
Radiation source: Mova (Mo) X-ray Source	4820 reflections with $I > 2.0\sigma(I)$
mirror	$R_{\text{int}} = 0.093$
Detector resolution: 15.9897 pixels $\text{mm}^{-1}$	$\theta_{\text{max}} = 29.2^\circ$ , $\theta_{\text{min}} = 3.1^\circ$
w scans	$h = -12 \rightarrow 13$
Absorption correction: analytical <i>CrysAlis PRO</i> , Agilent Technologies, Version 1.171.36.28 (release 01-02-2013 CrysAlis171.NET) (compiled Feb 1 2013, 16:14:44) Analytical numeric absorption correction using a multifaceted crystal model based on expressions derived by R.C. Clark & J.S. Reid. (Clark, R. C. & Reid, J. S. (1995). <i>Acta Cryst. A</i> 51, 887-897)	$k = -14 \rightarrow 14$
$T_{\text{min}} = 0.087$ , $T_{\text{max}} = 0.292$	$l = -15 \rightarrow 15$
18778 measured reflections	

### Refinement

Refinement on $F^2$	Primary atom site location: structure-invariant direct methods
Least-squares matrix: full	Hydrogen site location: difference Fourier map
$R[F^2 > 2\sigma(F^2)] = 0.042$	H-atom parameters constrained
$wR(F^2) = 0.104$	Method = Modified Sheldrick $w = 1/[\sigma^2(F^2) + (0.07P)^2 + 0.0P]$ , where $P = (\max(F_o^2, 0) + 2F_c^2)/3$
$S = 0.97$	$(\Delta/\sigma)_{\text{max}} = 0.001$
5210 reflections	$\Delta_{\text{max}} = 2.79 \text{ e } \text{\AA}^{-3}$
244 parameters	$\Delta_{\text{min}} = -3.66 \text{ e } \text{\AA}^{-3}$
0 restraints	

A Suitable crystal was selected and mounted on a Gemini kappa-geometry diffractometer (Agilent Technologies UK Ltd) equipped with an Atlas CCD detector and using Mo radiation ( $\lambda = 0.71073 \text{ \AA}$ ).

Intensities were collected at 100 K by means of the CrysAlisPro software. <sup>[1]</sup> Reflection indexing, unit-cell parameters refinement, Lorentz-polarization correction, peak integration and background determination were carried out with the CrysAlisPro software. <sup>[2]</sup> An analytical absorption correction was applied

using the modeled faces of the crystal. <sup>[3]</sup> The resulting set of hkl was used for structure solution and refinement.

The structures were solved by direct methods with SIR97 <sup>[4]</sup> and the least-square refinement on F2 was achieved with the CRYSTALS software. <sup>[5]</sup>

All non-hydrogen atoms were refined anisotropically. The hydrogen atoms were all located in a difference map, and then were repositioned geometrically. The H atoms were initially refined with soft restraints on the bond lengths and angles to regularize their geometry (C---H in the range 0.93--0.98 Å) and Uiso(H) (in the range 1.2-1.5 times Ueq of the parent atom), after which the positions were refined with riding constraints.

#### 4. TEM pictures of M-Ir and corresponding EDX analyses

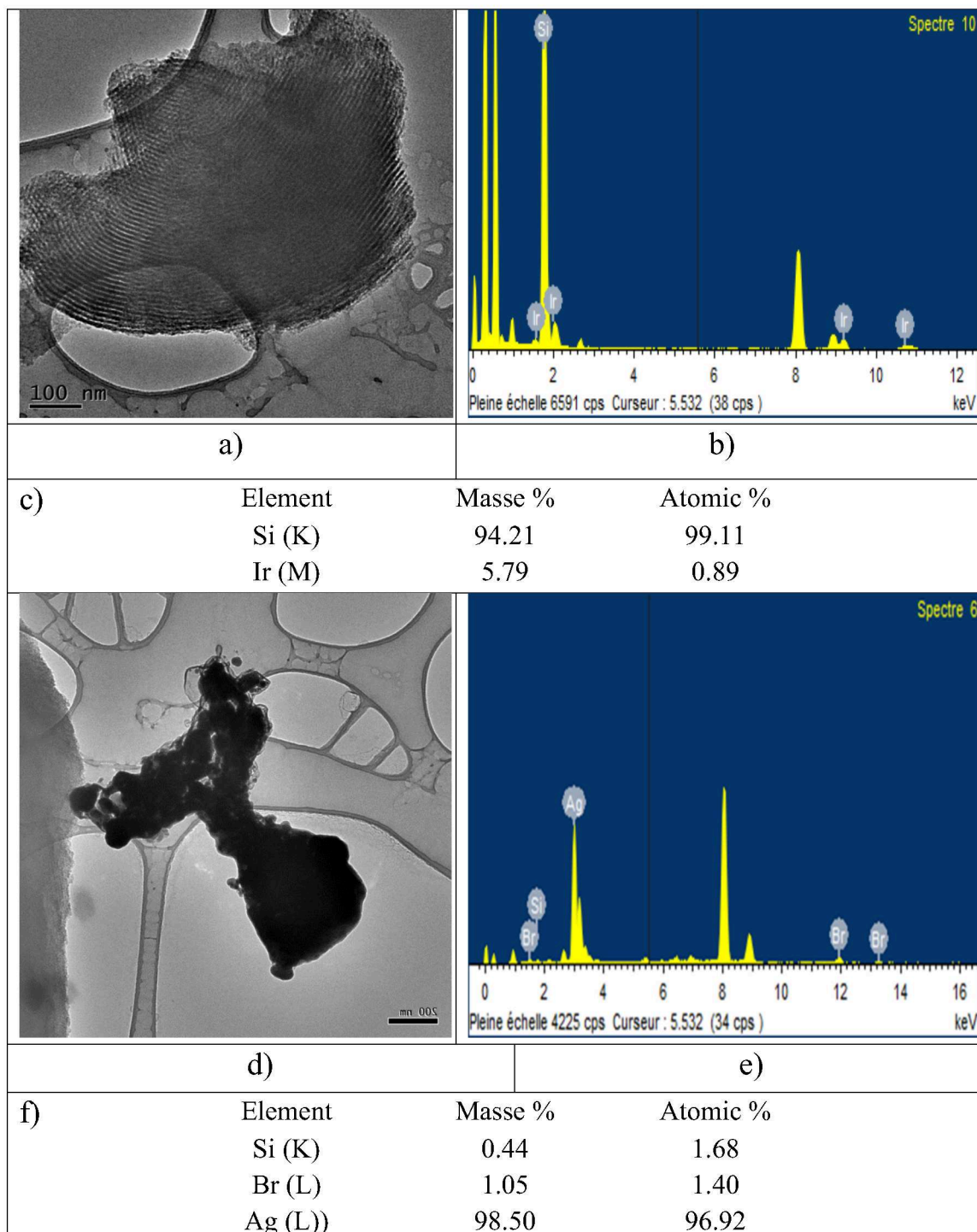


**Figure S7.** a) and d) TEM micrographs of **M-Ir**, b) and e) EDX spectra of respective regions, c) and f) element masse and atomic percent calculated from EDX spectra.

## 6. Synthesis and characterization of $^{13}\text{C}$ labelled materials

The synthesis of the  $^{13}\text{C}$  labelled-material was performed in the same way as for the non-labelled one by using  $\text{C}_2\text{-}^{13}\text{C}$ -labelled mesitylimidazole. **M-Im\***, **M\*-Ag**, **M\*-Ir** were prepared.

All labelled materials were characterized by conventional solid-state MAS-NMR spectroscopy. The experiments were carried out on a Bruker AVANCE III narrow bore spectrometer operating at a  $^1\text{H}$  Larmor frequency of 800 MHz using a 3.2 mm probe.

**TableS2. NMR parameters**

Materials	All	All	M-Im*	M*-Ag/M*-Ir
Pulse Sequence	Hahn Echo	CP/MAS	HETCOR	HETCOR
Nuclei	$^1\text{H}$	$^{13}\text{C}$	$^1\text{H}\text{-}^{13}\text{C}$	$^1\text{H}\text{-}^{13}\text{C}$
Number of scans	8	20480	1024	1152/1984
Recycle Delay (s)	10	2.0	2.0	2.0
Spinning rate (kHz)	22	22	22	22
Acquisition length (number of points)	3244	4096	5120	5120
$^1\text{H}$ 90° pulse width [ $\pi/2$ ] ( $\mu\text{s}$ )	2.5	2.5	2.5	2.5
Rotor period	1	-	-	-
Contact pulse length (ms)	-	2	0.5/2	2
$^1\text{H}$ rf field during contact pulse (kHz)	-	81	81	81
X rf field during contact pulse (kHz)	-	106	106	106
$^1\text{H}$ magic pulse width ( $\mu\text{s}$ )	-	-	1	1
$^1\text{H}$ rf field during eDUMBO decoupling (kHz)	-	-	100	100
Number of increments	-	-	64	74/72
Size of increments	-	-	32	64

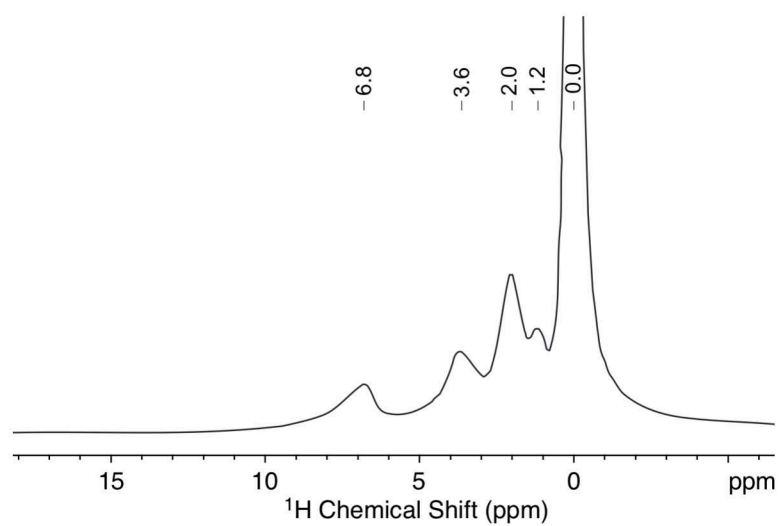


**Figure S8.** <sup>1</sup>H Hahn echo NMR spectrum of **M<sup>\*</sup>-Ir**.

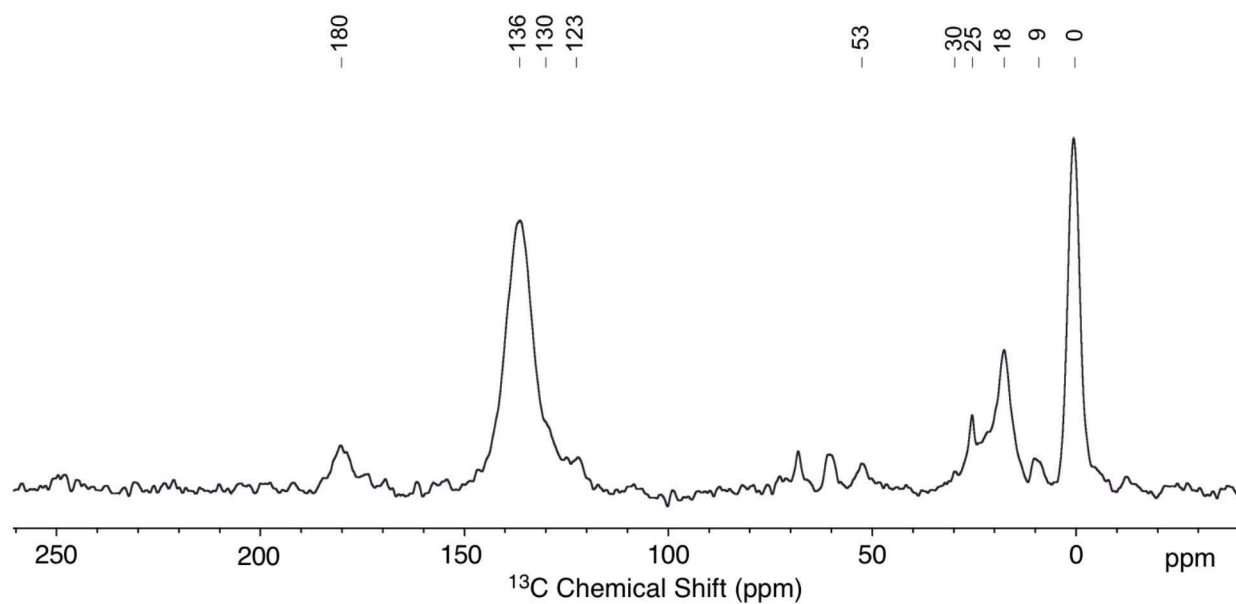


**Figure S9.** <sup>13</sup>C CP MAS NMR spectrum of **M<sup>\*</sup>-Ir**.

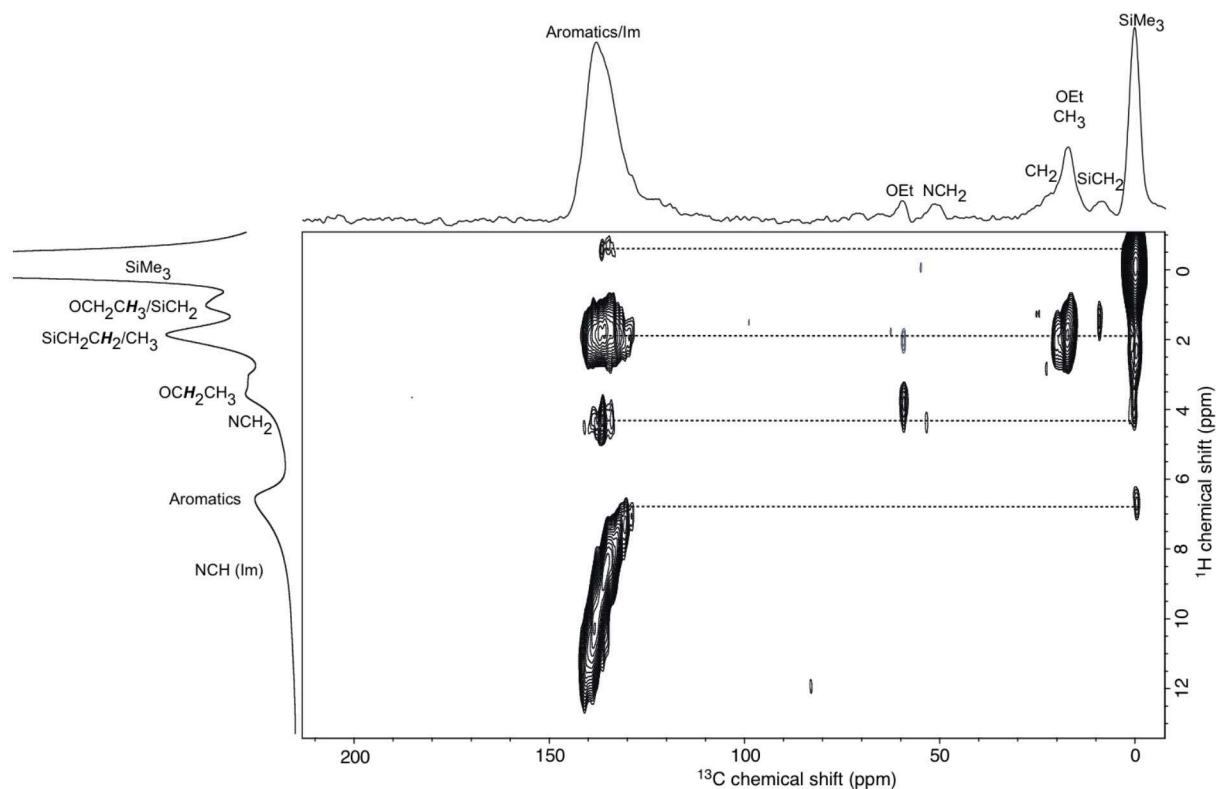


**Figure S10.**  $^1\text{H}$ - $^{13}\text{C}$  HETCOR NMR spectrum of  $\text{M}^*\text{-Im}$  with long distance correlations (contact time = 2 ms). The top trace is the corresponding 1D  $^{13}\text{C}$  CPMAS spectrum and the left trace the corresponding 1D  $^1\text{H}$  Hahn echo spectrum. Crosspeaks between protons of the TMS groups (0 ppm), of the  $\text{CH}_3$  of mesityl groups (2 ppm), and of the  $\text{NCH}_2$  moieties (4.2 ppm) with the aromatic carbons at 130 ppm are observed. Long-range correlations are shown by dashed lines.

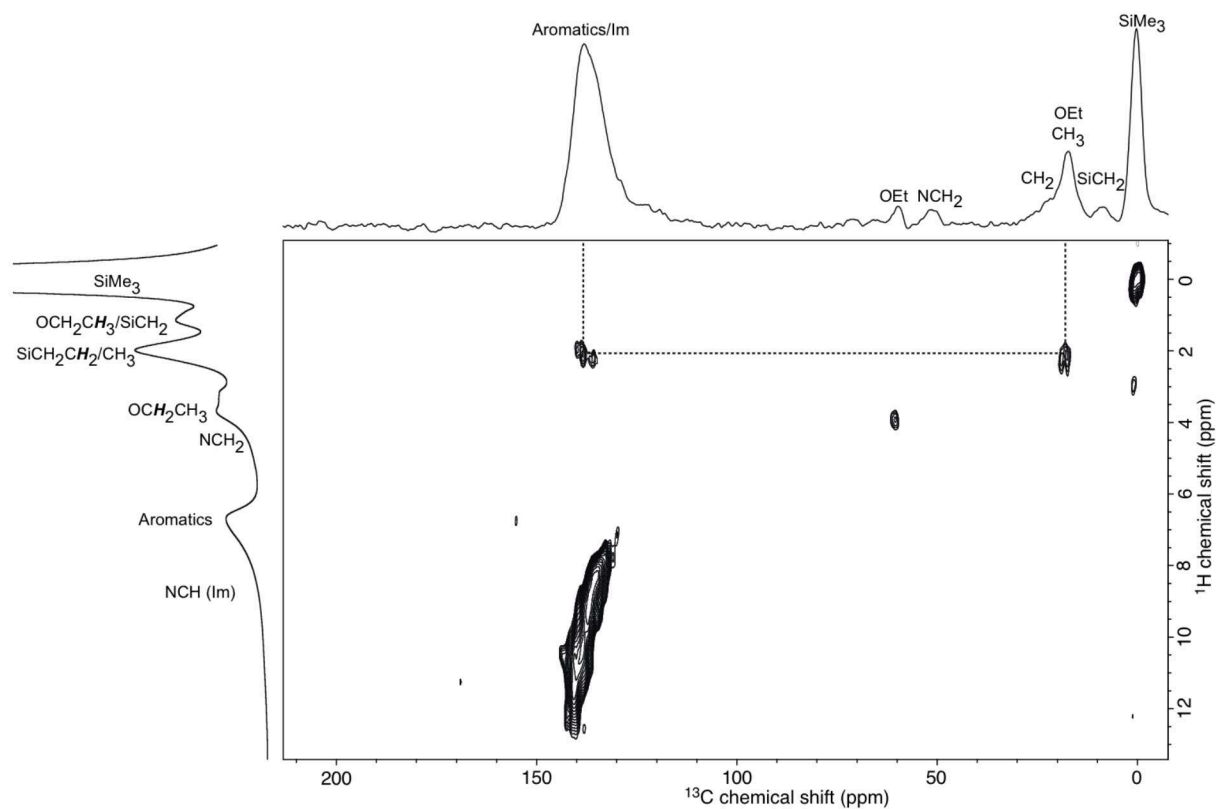


**Figure S11.**  $^1\text{H}$ - $^{13}\text{C}$  HETCOR NMR spectrum of M-Im\* with short distance correlations (contact time = 500  $\mu\text{s}$ ). The top trace is the corresponding 1D  $^{13}\text{C}$  CPMAS spectrum and the left trace the corresponding 1D  $^1\text{H}$  Hahn echo spectrum. The crosspeak at 140 ppm in  $^{13}\text{C}$  dimension and 2 ppm in  $^1\text{H}$  dimension correspond to (expected) spatial proximities between methyl substituents of mesityl and the aromatic part. Dashed line underlines these spatial interactions.

## 7. Characterization of Iridium(I) based NHC material by DNP method

10 mg of dry powder was wetted with 20 mL of 16 mM solution of bCTbK in 1,1,2,2-tetrachlorethane. The mixture was packed in 3.2mm sapphire rotor and quickly inserted in DNP spectrometer. The precise description of sample preparation can be found in our earlier articles.<sup>[2]</sup> Conditions applied for DNP measurements summarized in TableS3.

**TableS3. SENS DNP NMR parameters**

Pulse Sequence	CP/MAS	CP/MAS solid echo	CP/MAS	HETCOR Solid echo	HETCOR
Nuclei	<sup>13</sup> C	<sup>13</sup> C	<sup>29</sup> Si	<sup>1</sup> H- <sup>13</sup> C	<sup>1</sup> H- <sup>29</sup> Si
MW ON/OFF	MW ON/OFF	MW ON	MW ON/OFF	MW ON	MW ON
Number of scans	64	8192	32/64	128	128
Recycle Delay (s)	2.0	2.0	2.0	1.5	2.0
Spinning rate (kHz)	8	9	8	11	11
Acquisition length (number of points)	1608	4096	4096	810	718
<sup>1</sup> H 90° pulse width [ $\pi/2$ ] ( $\mu$ s)	2.5	2.5	2.5	2.5	2.5
Rotor period	-	40	-	25	-
Contact pulse length (ms)	1	2	6	0.5	0.2/2
<sup>1</sup> H rf field during contact pulse (kHz)	82	82	82	82	82
X rf field during contact pulse (kHz)	124	122	147	122	129
<sup>1</sup> H magic pulse width ( $\mu$ s)	-	-	-	1	1
<sup>1</sup> H rf field during eDUMBO decoupling (kHz)	-	-	-	100	100
Number of increments	-	-	-	128	128
Size of increments ( $\mu$ s)	-	-	-	64	64



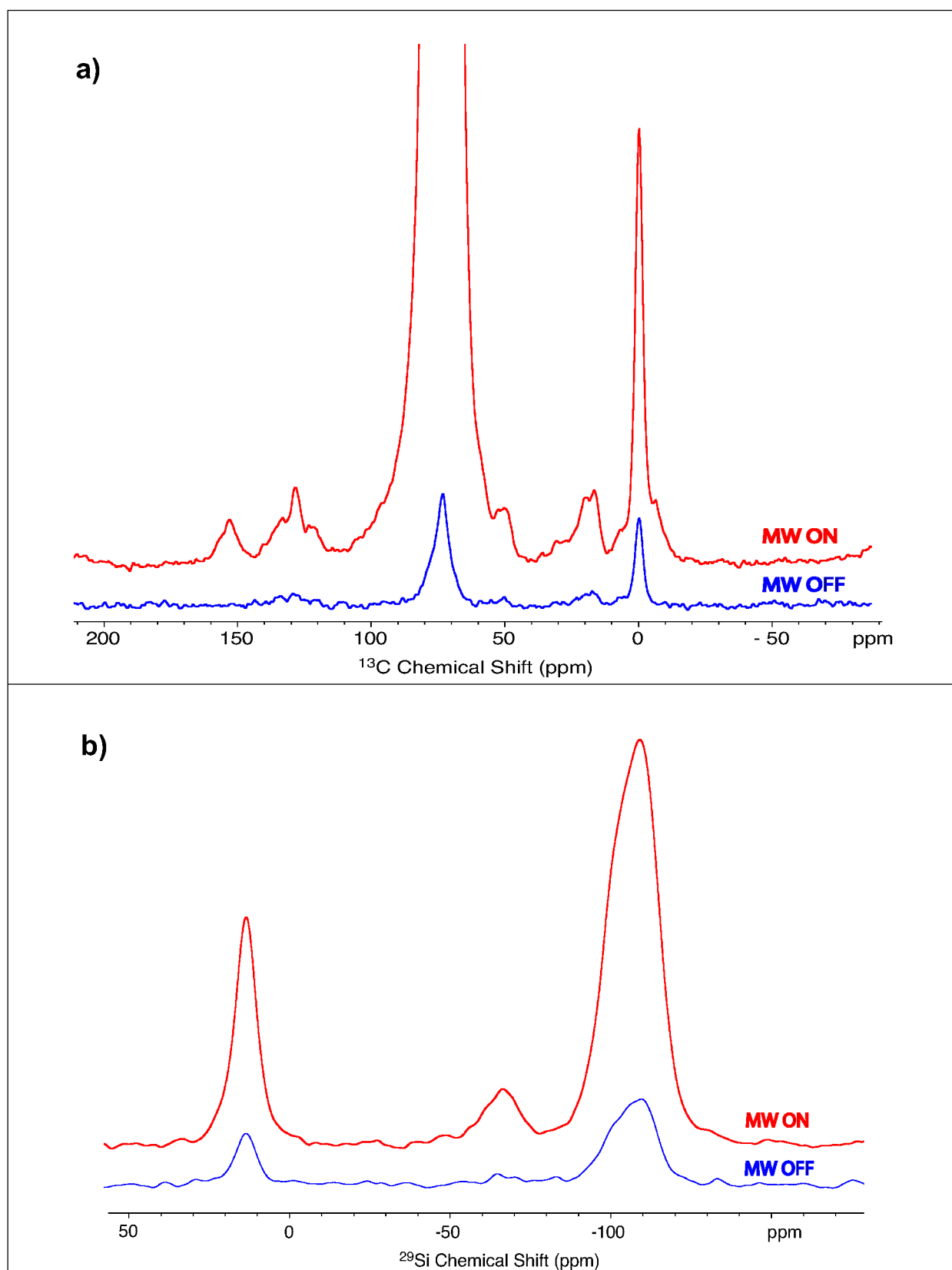


**Figure S12.**  $^{13}\text{C}$  (a) and  $^{29}\text{Si}$  (b) DNP MAS-NMR spectra of M-Ir recorded with mW irradiation on and off. The DNP enhancements were  $\epsilon = 5.1$  and  $\epsilon = 4.8$  for  $^{13}\text{C}$  and  $^{29}\text{Si}$  CPMAS spectra respectively.

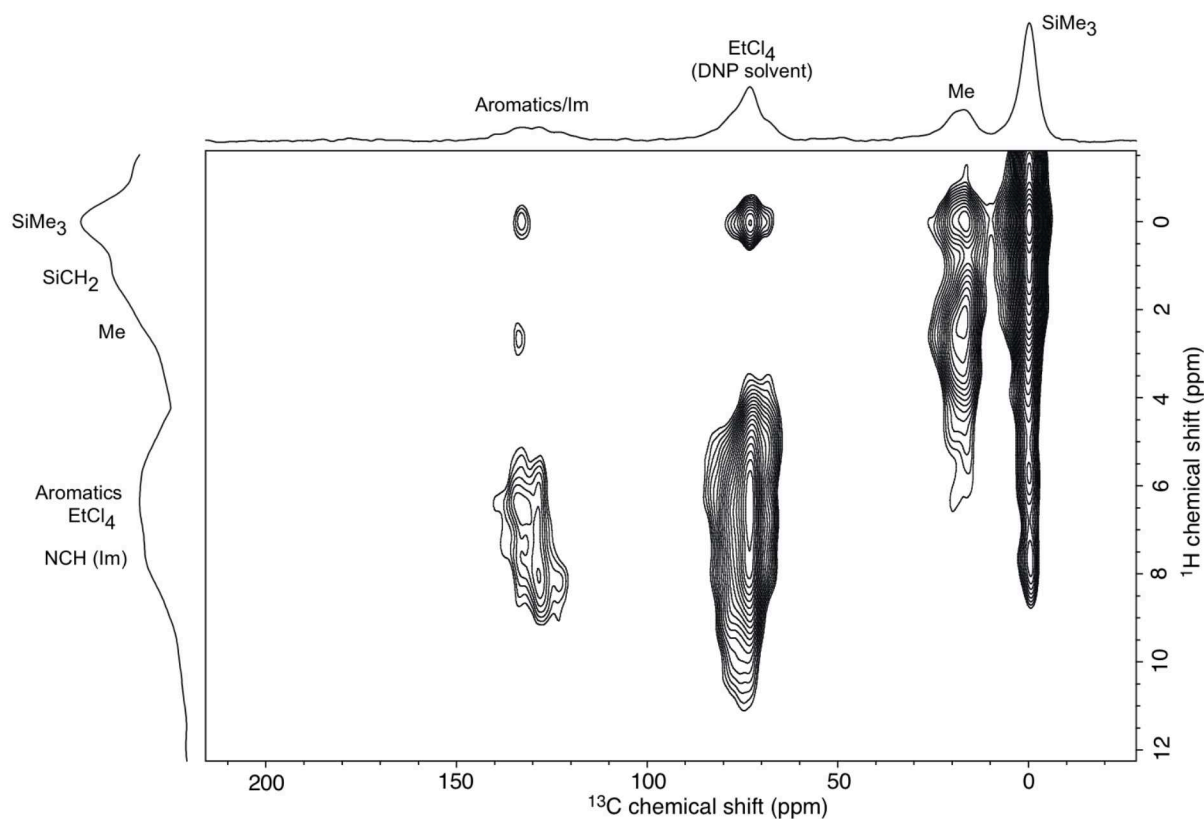


**Figure S13.** 2D  $^1\text{H}$ - $^{13}\text{C}$  HETCOR with solid echo (25 rotor periods) spectrum of **M-Ir** acquired with 0.5 ms contact time under DNP conditions. The top trace corresponds to the 1D  $^{13}\text{C}$  CPMAS solid echo spectrum and the left trace to the  $^1\text{H}$  internal projection (on the 1D  $^1\text{H}$  spectrum, only solvent is observable). Correlations at 50 ppm in  $^{13}\text{C}$  dimension and 3 ppm in  $^1\text{H}$  dimension as well as correlations at 25-35 ppm in  $^{13}\text{C}$  dimension and 5 ppm in  $^1\text{H}$  dimension corresponding to the  $\text{sp}^2$  and  $\text{sp}^3$  hybridized carbons of COD respectively could not be detected. However, the correlation between aromatic carbons at 140 ppm in  $^{13}\text{C}$  dimension and 0 ppm in the  $^1\text{H}$  dimension (TMS protons) as well as correlations at 0 ppm in  $^{13}\text{C}$  dimension with 7-10 ppm in  $^1\text{H}$  dimension suggest the folding of organic functionalities onto the surface, as observed already with conventional solid-state NMR spectroscopy.

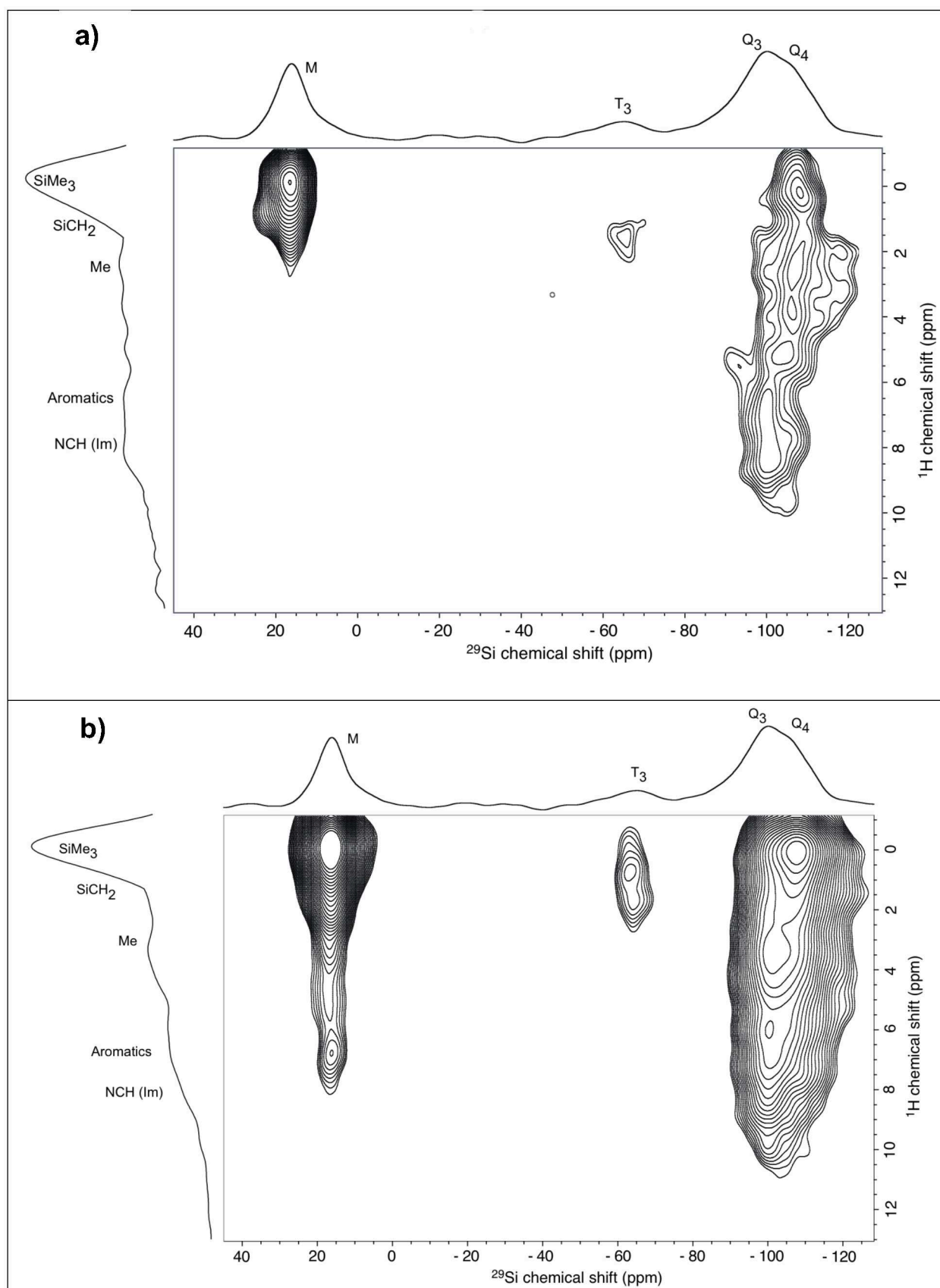


**Figure S14.** 2D  $^1\text{H}$ - $^{29}\text{Si}$  HETCOR spectra of **M-Ir** acquired with short (0.2 ms, **a**) and long (2.0 ms, **b**) contact times under DNP conditions. The top traces correspond to the 1D  $^{29}\text{Si}$  CPMAS solid echo spectrum and the left traces to the

$^1\text{H}$  internal projection (on the 1D  $^1\text{H}$  spectrum, only solvent is observable). Crosspeaks at 20 ppm in  $^{29}\text{Si}$  dimension and 2-7 ppm in  $^1\text{H}$  dimension are assigned to spatial proximities between the TMS groups and the organic functionalities (2CH<sub>3</sub> of mesityl at 2 ppm, NCH<sub>2</sub> at 4 ppm, aromatic protons at 7 ppm), illustrating again the folding of the organic functionalities onto the surface.

## 8. NMR experiments under H<sub>2</sub> pressure for COD concentration determination

The detection of cyclooctane release from material was performed in high pressure stable (up to 7 bars) QVP NMR tube. The NMR tube is prepared under inert atmosphere, with 36 mg of material **M-Ir** (0.006 mmol of Ir), 2.8 ml of dry degased C<sub>6</sub>D<sub>6</sub> and 10  $\mu\text{L}$  (0.094 mmol) of dry degased toluene as a standard. The tube was then pressurized under 3 bars of H<sub>2</sub> and the reaction was monitored by  $^1\text{H}$  NMR at 25 °C. The appearance of a signal at 1.5 ppm corresponding to cyclooctane product was detected (Figure S16). No more release of cyclooctane was detected after 27 h reaction. To confirm the cyclooctane formation 0.5  $\mu\text{L}$  of pure cyclooctane was added to the NMR tube (Figure S16).

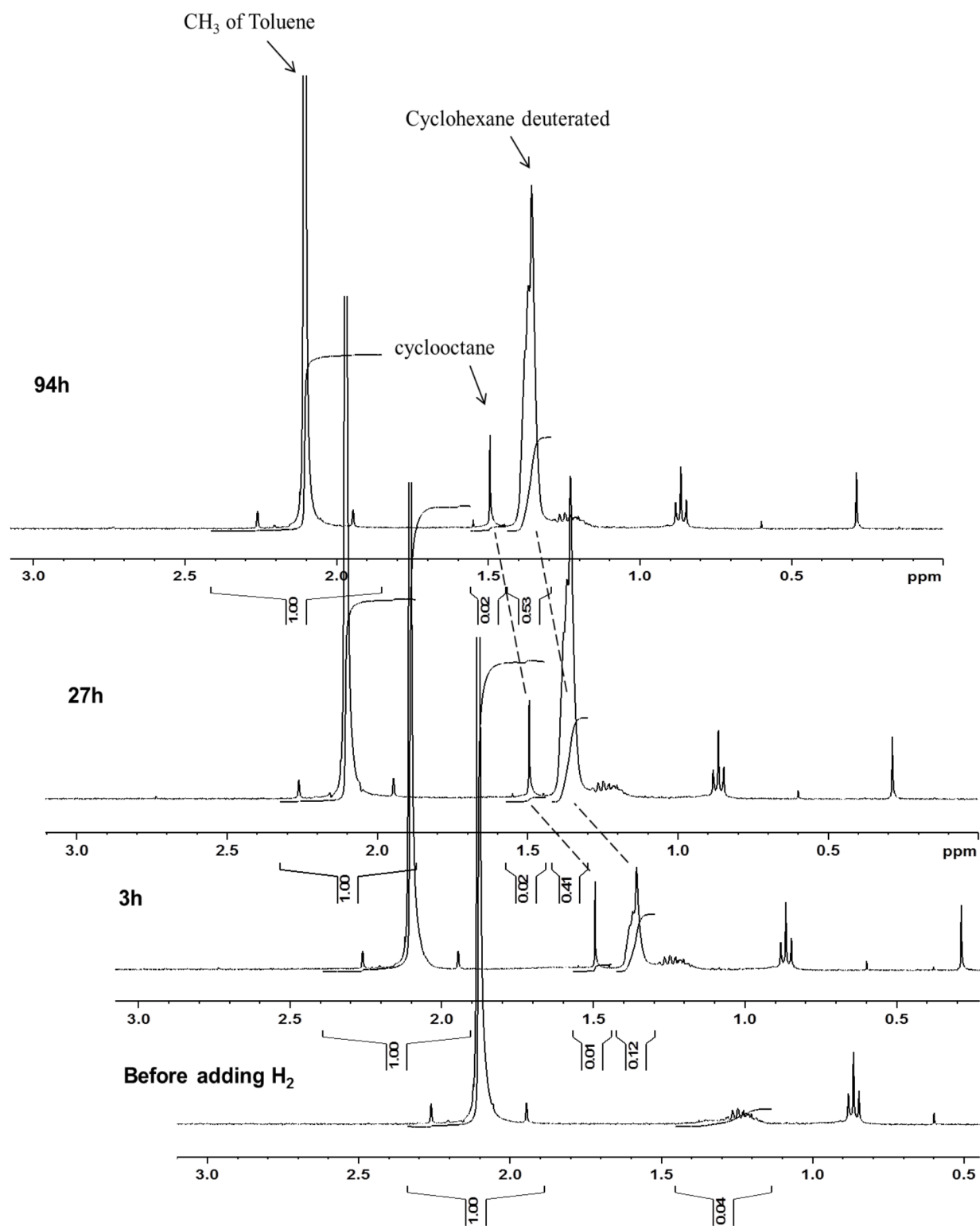


**Figure S15.** *In situ*  $^1\text{H}$  NMR detection of cyclooctane ( $\text{C}_6\text{D}_6$ , 300K; 400MHz)

Beside the evolution of cyclooctane (1,5 ppm), the hydrogenation of  $\text{C}_6\text{D}_6$  is observed, as shown by the growth of a broad signal at ca. 1.37 ppm, corresponding to deuterated cyclohexane. This result suggests the formation of Ir NPs during the experiment thus showing that such NPS are only formed

when no olefinic substrate is present. This result is further confirmed by TEM micrographs and EDX performed on the recovered material after 94h under H<sub>2</sub> in C<sub>6</sub>D<sub>6</sub> (See fig. S17).

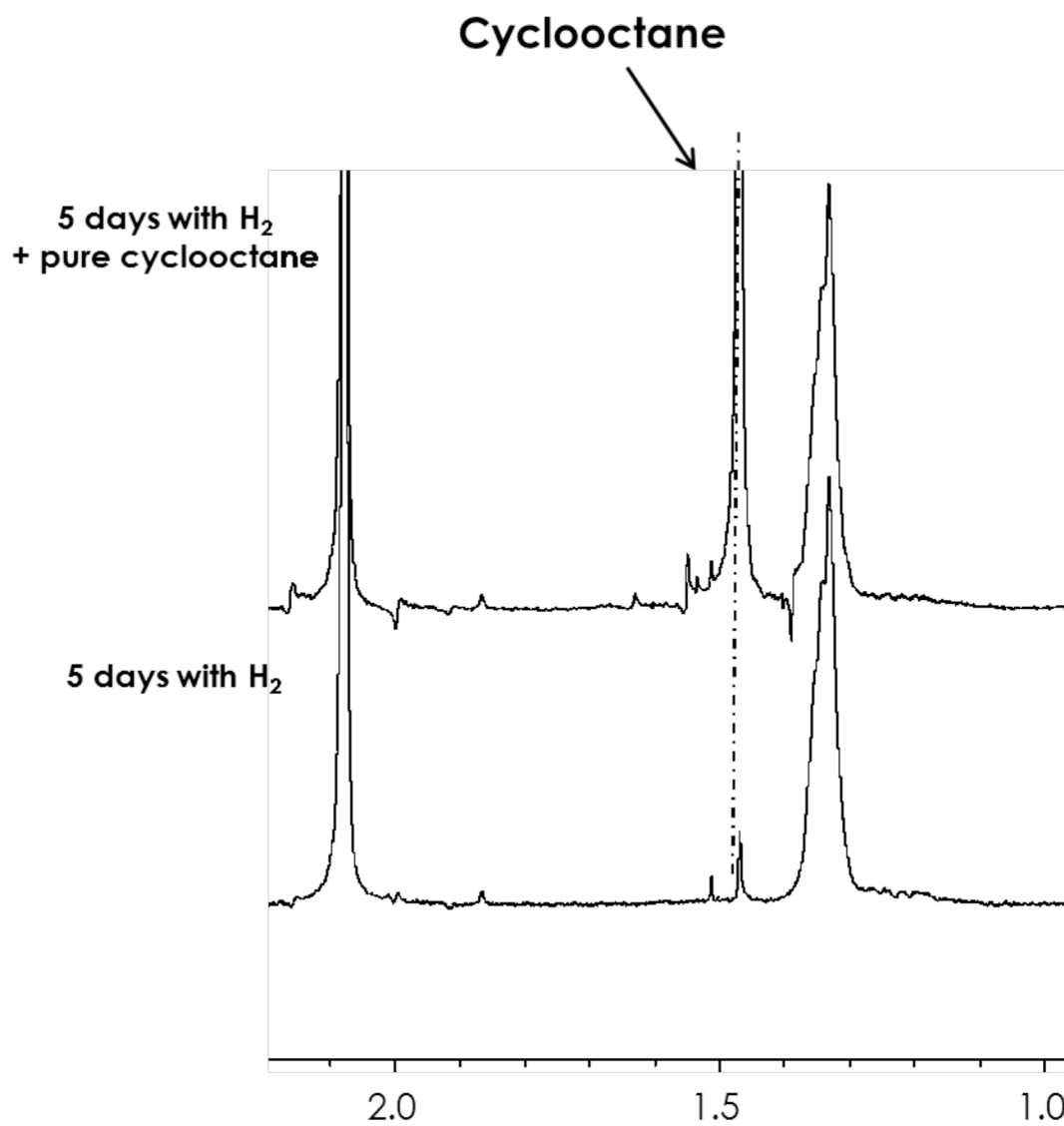


**Figure S16.** <sup>1</sup>H NMR detection of cyclooctane (C<sub>6</sub>D<sub>6</sub>, 300K; 300MHz)

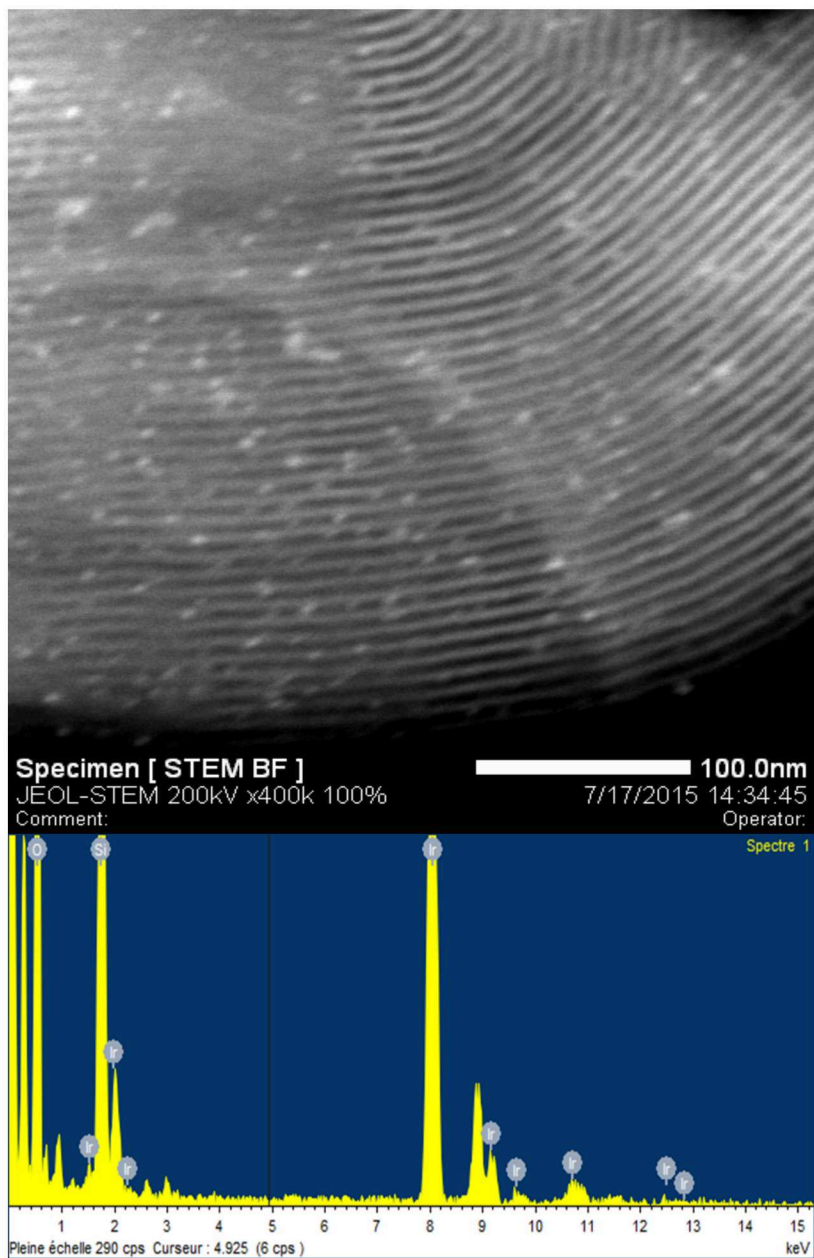


**Figure S17.** STEM micrograph and EDX of the recovered solid after 94 hours under H<sub>2</sub> in C<sub>6</sub>D<sub>6</sub> and toluene as internal standard.

## 9. Procedures for catalytic experiments with homogeneous [IrCl(COD)(MesImPr)], [Ir(COD)(MesImPr)]BF<sub>4</sub> and heterogeneous Iridium(I) based NHC material

All the tests were performed in specifically adapted glass reactor with connection to vacuum, argon and hydrogen lines. The catalyst, substrates and internal standard were introduced into the reactor under argon using standard Schlenk techniques. Trans-stilbene was received from Sigma-Aldrich and was recrystallized from methanol prior to use. Before each catalytic test, reactor was purged with Argon. The catalysis performed with 0.1 mol% of catalyst (corresponding to Ir) at 40 °C under 3 bars of H<sub>2</sub> pressure. Reaction was monitored by <sup>1</sup>H NMR. The conversion was measured by relative disappearance of peak at 3.78 ppm which corresponds to =CH of double bond and appearance of peak at 2.98 ppm which corresponds to -CH<sub>2</sub> of hydrogenated product. 1, 2-tetrachloroethane was used as internal standard.

### Heterogeneous catalysis

10 mg of **M-Ir** (0.0017 mmol of Ir) were mixed in a glove box with 300 mg of trans-stilbene (1.67 mmol). The mixture was dissolved in 3.5 ml of dry degassed toluene. 0.1ml of internal standard was added and all mixture was transferred to glass reactor (reactor volume=30 mL) with the help of cannula.

For the determination of maximum TON was used more diluted system (0.01mol% of catalyst). 60mg of M-Ir (0.005 mmol of Ir, batch with 25% silver to iridium conversion) were mixed in glove box with 8.460g of trans-stilbene (47 mmol). The mixture was dissolved in 85mL of dry degassed toluene. 0.5ml of internal standard was added and all mixture was transferred to glass reactor (reactor volume=400mL) with the help of cannula.

### Homogeneous catalysis

752 μL of 0.022 M solution of [IrCl(COD)(MesImPr)] (0.017 mmol) was introduced in a Schlenk already containing 3 g of trans-stilbene (16.7 mmol) dissolved in 35 mL of dry degassed toluene. After 0.2 ml of internal standard were added. The mixture was transferred to glass reactor (reactor volume=300ml) with the help of cannula.

The cationic species [Ir(COD)(MesImPr)]BF<sub>4</sub> was generated *in situ* with addition of 0.0017 mmol of AgBF<sub>4</sub> (300 μL of dry degassed 0.056 M solution in



toluene) inside the glass reactor (reactor volume=300ml) before pressurizing with H<sub>2</sub>. It was seen the precipitation of white solid of AgI.

### **Scope of substrates**

Styrene and its derivatives with electron donating (4-vinylanisole, 4-acetoxystyrene) and election withdrawing (4-fluorostyrene) substituents were chosen as substrates for hydrogenation. The substituted styrenes were received from Sigma-Aldrich and dried with 5 Å molecular sieves prior to use. Transstilbene was used as a bench mark and was purified as previously described. The catalysis performed in toluene with 0.03 mol% of catalyst loading (corresponding to Ir) at 40 °C under 3 bars of H<sub>2</sub>.

10 mg of M-Ir (0.0017 mmol) were suspended at 10ml of dry degased toluene. Solution was transferred in the reactor under Argon. 5.1mmol of Substrate was then introduced followed by addition of 0.1 mL of the internal standard.

Homogeneous and heterogeneous catalytic experiments were performed with similar conditions [IrCl(COD)(MesImPr)] was introduced as 1.4 mL of 0.001M stock solution and 8.5 mL of solvent was added.

Reactions were monitored by <sup>1</sup>H NMR. The results are presented in Figure S18 and in Table S4.

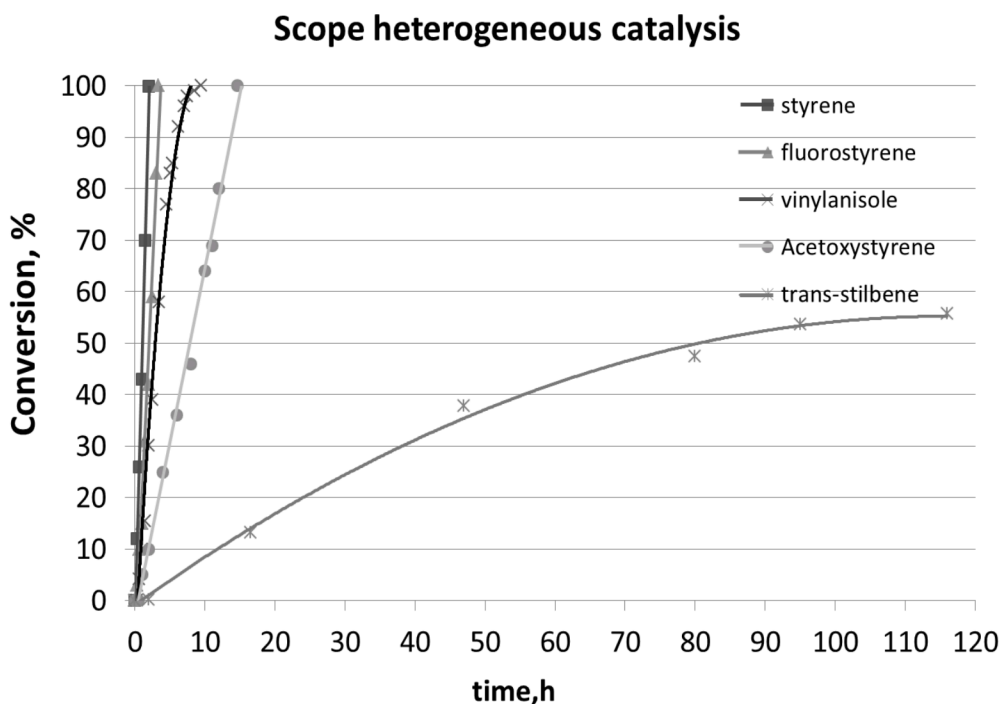


**Figure S18.** Scope of substrates for **M-Ir**. Conversion of alkene (%).

**TableS4. Comparison of TOF ( $\text{h}^{-1}$ ) for homogeneous and heterogeneous catalysts**

Substrate	TOF, $\text{h}^{-1}$		Improvement
	M-Ir	[IrCl(COD)(MesImPr)]	
styrene	1400	177	8 times faster
4-fluorostyrene	750	170	4.5 times faster
4-vinilanisole	190	120	4 times faster
4-acetoxystyrene	490	125	1.5 times faster
<i>trans</i> -stilbene	44	4	10 times faster
limonene	125	20	6 times

For Styrene's derivatives, the TOF ( $\text{h}^{-1}$ ) was calculated at 50 % conversion. For *trans*-stilbene, the TOF ( $\text{h}^{-1}$ ) was calculated at 50 h of reaction.

### Split tests

#### *Leaching of active species:*

After full conversion of substrate (acetoxystyrene), the supernatant was collected and filtered under Ar and portion of substrate (limonene) was added. No conversion of limonene was detected during 30h (Fig. 19).

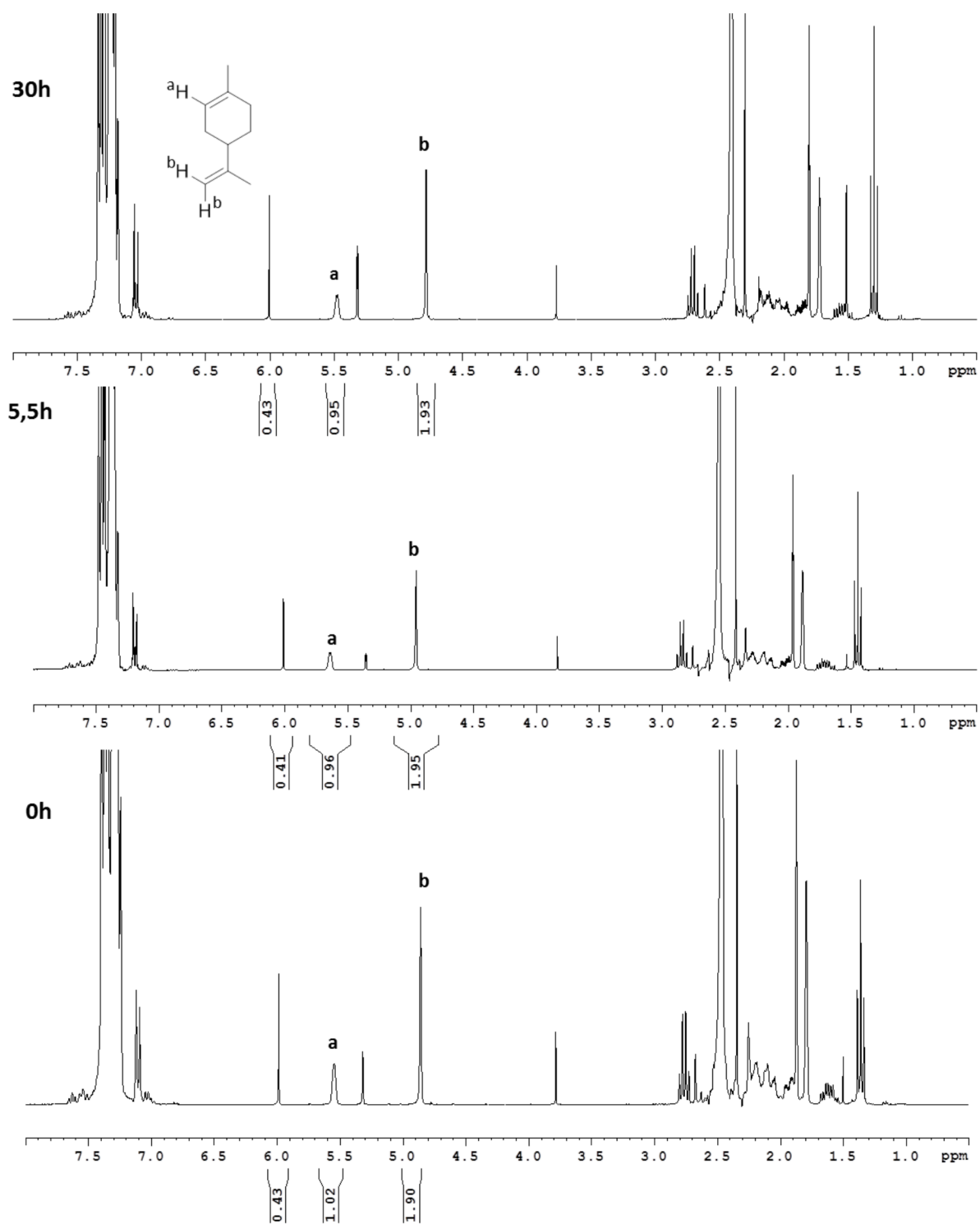


**Figure S19.**  $^1\text{H}$  NMR spectra of limonene hydrogenation by recovered supernatant from acetoxystyrene hydrogenation

*Leaching of inactive species:*

After full conversion of substrate, the supernatant was collected and separate from **M-Ir** by filtration and send to elemental analysis.. According to the results, the detected Ir leaching is less than 1ppm.

### References

- [1] T. K. Maishal, J. Alauzun, J.-M. Basset, C. Copéret, R. J. P. Corriu, E. Jeanneau, A. Mehdi, C. Reyé, L. Veyre, C. Thieuleux, *Angew. Chem. Int. Ed.* **2008**, 47, 8654-8656.
- [2] CrysAlisPro, Agilent Technologies, Version 1.171.34.49 (release 20-01-2011 CrysAlis171 .NET) (compiled Jan 20 2011,15:58:25)
- [3] R. C. Clark & J. S. Reid, *Acta Cryst. A* **1995**, 51, 887-897.
- [4] A. Altomare, M.C. Burla, M. Camalli, G.L. Cascarano, C. Giacovazzo, A. Guagliardi, A. Grazia, G. Moliterni, G. Polidori, R. Spagna, *J. Appl. Cryst.* **1999**, 32, 115-119.
- [5] P.W. Betteridge, J.R. Carruthers, R.I. Cooper, K. Prout, D.J. Watkin, *J. Appl. Cryst.* **2003**, 36, 1487-1487.
- [6] M. P. Conley, R.M. Drost, M. Baffert, D.Gajan, C.Elsevier, W. T. Franks, H. Oschkinat, L.Veyre, A. Zagdoun, A. Rossini, M. Lelli, A. Lesage, G. Casano, O. Ouari, P. Tordo, L. Emsley, C. Coperet, and C. Thieuleux. *Chem. Eur. J.* **2013**, 19, 12234-12238.